UNIVERSITY of CALIFORNIA
SANTA CRUZ

A CASE STUDY ON THE NATURE OF PLANET-LIKE AND STAR-LIKE FORMING OBJECTS: THE PHOTOMETRY OF PLANETS AND BROWN DWARFS

A thesis submitted in partial satisfaction of the requirements for the degree of

BACHELOR OF SCIENCE

in

ASTROPHYSICS

by

****

June 11, 2012

_____ _____

********** **********

Advisor Senior Theses Coordinator

_____

****

Chair, Department of Physics

Abstract

A Case Study on the Nature of Planet-like and Star-like Forming Objects:
The Photometry of Planets and Brown Dwarfs

by

****

I present a method to contrast the characteristics of extrasolar planet and brown dwarf atmospheres through photometry, as well as a means to better understand these two very different types of objects. I have compiled together all the known planetary and brown dwarf photometric data at the 3.6μm, 4.5μm, 5.8μm, and 8.0μm wavelength bands observed on the *Spitzer Space Telescope* and the *Wide-Field Infrared Survey Explorer*. This data set currently contains 30 unique and exotic extrasolar gas giant planets, as well as 210 known brown dwarfs. These objects range from effective temperatures of 200-3000K, and exhibit many different stages of evolution. I will describe, in detail, the formation and chemical structure of gas giant planets and brown dwarfs, and how these relate to the relationships that we see among color, temperature, and radius in planets and brown dwarfs. To exhibit these trends, I have constructed a number of characteristic profiles, including a pressure-temperature profile, six color-temperature profiles, and six radius-color-temperature "diversity" profiles. These profiles present a striking picture of gas giant planet diversity that contrasts the steady and consistent chemical evolution of brown dwarfs.

Contents

List of Figures

List of Tables

Acknowledgements

I want to thank first and foremost my thesis advisor, *********, for guiding me in the majority of this research project over the span of my internship, and being available for assistance whenever I needed it. I also want to thank my thesis coordinator and professor, **********, for giving me guidance in the early stages of writing my thesis, as well as providing me advice and reassurance for graduate school throughout. This is my first full-fledged endeavor into a real scientific paper, and it has been an enjoyable and enlightening experience to work on it. Lastly and most importantly, I'd like to thank my parents, ********** and ********** for being supportive of me and my interests in astronomy throughout my life, without which, I wouldn't be where I am today.

I. Introduction

When Pluto was demoted to "dwarf planet" in mid-2006, astronomers and kindergarteners alike cried out in shock. Since its discovery close to a century ago, it had always been considered the ninth and last of the planets. This was brought into question when a larger object, Eris, was discovered on a rather eccentric orbit that stretched from around Pluto's orbit out to three times the orbital distance of Neptune (Brown et al. 2005). Soon thereafter, the classifications of twelve other similar objects were brought into question as well. It became apparent that we needed to find a more concrete definition for what a planet actually *was*. In response to the controversy, the International Astronomical Union (IAU) defined a solar system planet under three axioms: 1) it must be orbiting around the sun, 2) it must be massive enough to reach hydrostatic equilibrium and be roughly spherical in shape, and 3) it must have cleared out the surrounding area of other major orbiting bodies.

This definition has since held, despite much controversy and criticism. Six years later, the public eye has shifted to the hundreds of discoveries regarding extrasolar planets. We have detected planets of all kinds orbiting around a variety of other stars, ranging from sun-like to red dwarfs, pulsars, and white dwarfs. Some of these planets have completely defied our expectations. We've found planets such as HD 209458b (Charbonneau et al. 1999), which orbits so close to its parent star that its atmosphere is evaporating away (Linsky et al. 2010). We've also found TrES-2b (O'Donovan et al. 2006), which is the darkest planet ever discovered, with an extremely low day to night contrast amplitude (Kipping et al. 2011). And then there is CoRoT-3b (Deleuil *et al. 2008*), which is over twenty times the mass of Jupiter, massive enough that most consider it to be a class of object known as a brown dwarf.

Brown dwarfs are sub-stellar objects that are typically massive enough to fuse deuterium and sometimes lithium. However, they are not massive enough to begin sustained fusion of hydrogen, and are therefore not considered a true main sequence star. Their masses can range from a large gas giant planet's (around 10-20 Jupiter masses), to that of a small red dwarf star (the least massive type of main sequence star, around 70-80 Jupiter masses). Many brown dwarfs have been discovered both on their own and orbiting parent stars. Some are low enough in mass and radius that they are hard to distinguish from a massive gas giant planet. As shown in Figure 1, even massive objects like CoRoT-3b are almost equivalent in size with Jupiter.

The IAU has currently worked out a temporary definition that dictates that objects below 13 Jupiter masses (the calculated limiting mass for deuterium fusion in an object with the sun's metallicity) should be considered planets, and those above be considered brown dwarfs. It also states that all objects floating freely in space below this limit should be considered "sub-brown dwarfs." Other definitions use larger limiting masses, such as that used by the Extrasolar Planet Encyclopedia (EPE), which places the dividing line around 25 Jupiter masses (thus including the aforementioned CoRoT-3b as a planet). For the time being, the majority of discoveries are designated by one of these classifications.

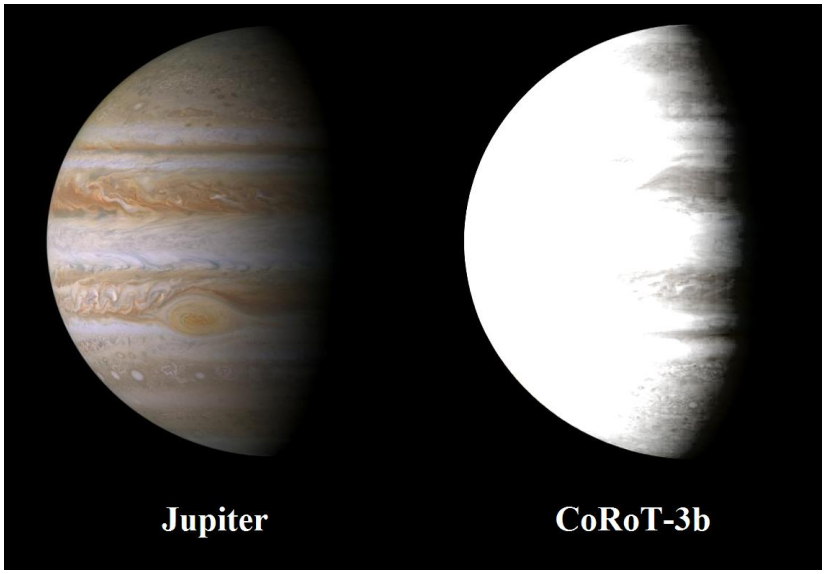

FIG. 1: As seen here, CoRoT-3b, although twenty times the mass of Jupiter, is only ~1.01 Jupiter radii. Figure based on Jupiter Image Source: *PIA04866: Cassini Jupiter Portrait,* NASA/JPL/Space Science Institute.

A key defining difference between brown dwarfs and planets overlooked by the mass-limit definitions is their formation. While planets form out of the gas and dust swirling around in the protoplanetary disk of a forming star, brown dwarfs form out of giant molecular clouds, but simply do not gather enough mass to begin sustained hydrogen fusion. Because of this, the difference between the two classes of objects lies within their interiors. This makes it particularly difficult to distinguish between the two, since they can be identical in terms of mass, radius, and can both be found in similar environments. However, we can obtain hints of the interior by looking at how the planet appears in certain wavelengths compared to other wavelengths.

An object's spectrum can help us in many ways to understand it. One way to measure this is the color index (magnitude in one wavelength minus another), which can yield some interesting insight into its nature. In this case, different chemical processes can have diverse effects on the color. By looking at how color varies with temperature, we can see that colder objects, which undergo a different set of atmospheric processes, may appear "bluer" or "redder" than warmer objects. Because we would expect to see some fundamental atmospheric differences in objects of star-like and planet-like formation, brown dwarfs and large gas giant planets should exhibit differing trends in color as they vary with effective temperature (the surface temperature of the object assuming that it is a "blackbody," an entirely non-reflective object), due to the differing chemical processes within. With this in hand, I will present a method of distinguishing brown dwarfs and planets based on their color and internal structure.

In the following two sections, I will discuss the nature of brown dwarfs and large gas giant planets, as well as the methods and background regarding measuring the flux ratios of planet-star systems. In Section IV, I will describe the method I used to obtain color indices from the planet-star flux ratio data and create our color-temperature and pressure-temperature profiles. In Section V, I will present all the data obtained from this project, and discuss the differences in

trends seen among planets and brown dwarfs. Section VI will discuss the conclusions reached based on this data, using color as a method of differentiation between brown dwarfs and planets, and the future implications of this method as more planet data is collected.

II. The Nature of Planets & Brown Dwarfs

IIa. Formation

Our understanding of extrasolar planets and brown dwarfs has expanded greatly over the past twenty years. While physical confirmation of these objects only came about in the early 1990s, speculation on their nature has been around for decades, and in the case of extrasolar planets, centuries. Following the footsteps of Copernicus, Giordano Bruno first postulated in 1584 that our solar system was not unique in having planets, and in the vast infinity there must exist many other planets orbiting around the stars that speckled the night sky. Quite simply: "*since it is well that this world doth exist, no less good is the existence of each one of the infinity of other worlds."* Of course, poor Bruno was quickly imprisoned and then burned at the stake for such ludicrous and unbounded heresy.

It wouldn't be until four hundred years later that tangible evidence to Bruno's claims would appear. The first handful of extrasolar planets to be confirmed were unlike anything seen before. The closest analogue in our solar system that astronomers could compare them to was Jupiter. However, these gas giant planets orbited unbelievably close to their parent star, well within the orbital distance of Mercury. These types of planets were thereafter referred to as "Hot Jupiters." Since then, a colorful planetary compendium has grown, including planets of all sizes, orbits, temperatures, and compositions. Understanding the origin of this vast diversity is the most important factor in recognizing how they differ from brown dwarfs and star-like objects in general.

Star and planet formation is an incredibly dynamic and beautiful process, and is primarily responsible for the overall diversity seen among planets. The story of planet formation begins with that of their parent star. For all stars, as well as brown dwarfs and other star-like objects, this begins in an enormous molecular cloud that can stretch across a hundred, if not several hundred, light-years. These clouds are scattered across the interstellar medium throughout the galaxy, and are thought to form from the natural contraction of interstellar gasses, sometimes fueled by the expelled gasses of an exploded supermassive star. Since these clouds are non-uniform, denser pockets of gas naturally occur within the cloud itself. Under the ever-present influence of gravity, these denser pockets gather together more material, becoming even denser, and more massive.

It is here that we see the slow "birth" of a protostar. As the gas heats up, the gas begins to radiate on the infrared spectrum deep within the interior of the cloud. However, this glow is obscured by the vast amounts of gas and dust that continue to gather around the protostar, making it rather difficult to detect by any practical means until much later in its formation. As the interior pressures steadily increase, the gas is forced into convection to stabilize itself. However, due to the sheer mass of molecular gas that is collecting, dissociating, and ionizing, the protostar will continue to heat up. This is when the would-be star begins to take on a personality.

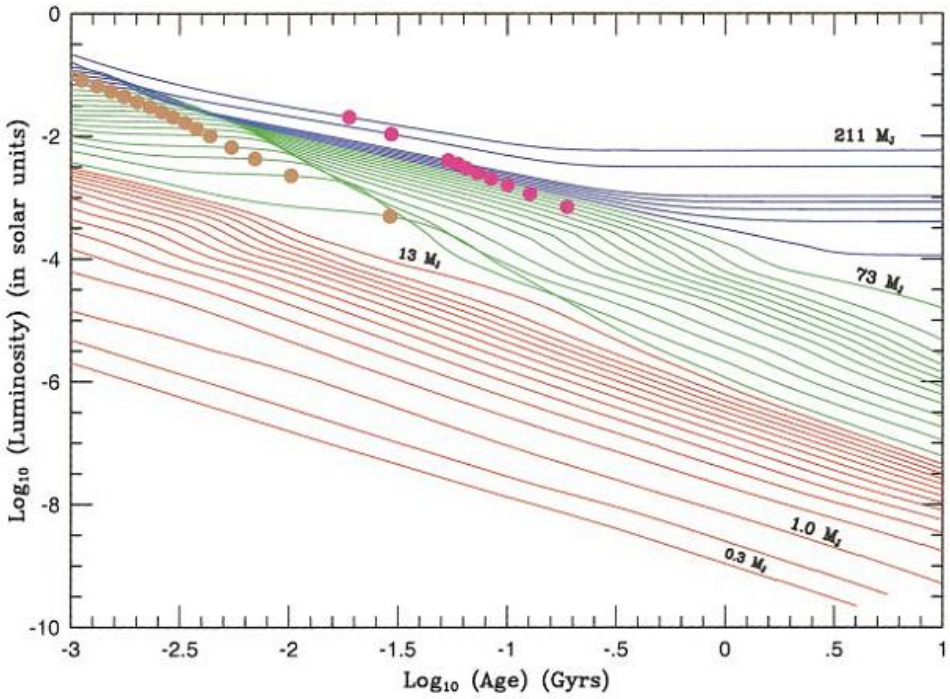

FIG. 2: The luminosities of star-like forming objects of various masses (ranging from 0.3 M_J to 211 M_J) are shown here as they evolve over time. Hydrogen fusing objects are shown in blue, deuterium fusing objects are shown in green, and objects with no fusion present are shown in red. By the IAU definitions, these would be red dwarfs, brown dwarfs, and sub-brown dwarfs respectively. The orange dots mark the point where 50% of the object's deuterium supply has been fused. Similarly, the magenta dots mark the point where 50% of the object's lithium supply has been fused. The objects shown in blue begin hydrogen fusion at around 0.1 to 3 Gyrs, (Burrows et al., 2001).

Depending on how much mass was in this particular pocket of the molecular cloud, the protostar may or may not have gained enough heat to ignite thermonuclear fusion, the main driving force behind all stars. In the case of our sun, a relatively modest yellow dwarf star, there was enough mass to begin fusion of hydrogen. From the point of ignition, this is referred to as a main sequence star. However, in many cases, there simply isn't enough mass to generate sufficient heat for this to happen. In these cases, we get an object that is more or less only heated by contraction, and this is typically what we call a brown dwarf. The hottest of the brown dwarfs are capable of fusing hydrogen; however, they are still not hot enough to sustain this fusion for very long. In most other cases, for a period of time early in their lifespan, they instead fuse deuterium or "heavy hydrogen." However, this too soon ceases when the deuterium supply is exhausted, leaving the brown dwarf to dim, cool, and contract until it is virtually undetectable, in contrast to red dwarf stars, which have a fairly constant luminosity after hydrogen burning begins, as shown in Figure 2.

For planets, the story gets a little more complex. The sufficient presence of heavier elements, referred to as "metals" (which by astronomer's terms, means anything heavier than hydrogen and helium), often, if not always, leads to planet formation. These heavier elements only arise from the ejecta of stars that fused these elements and then went supernova. Due to the contraction of all this gas and dust, the system as a whole begins to noticeably rotate, under the influence of angular momentum. As the system spins, the debris along the axis of rotation

contracts and spreads out into a large disk shaped cloud, much like a cook may toss and spin dough to form a pizza crust. These are known as protoplanetary disks, which are the first observable sign of planet formation.

As the disk stretches and thins, we begin to see a similar process to what we saw in early stellar formation. Denser clusters of dust naturally form within the disk, and begin to gather together more debris from the surrounding area under the influence of gravity. However, instead of just gas contracting, as was the case with the protostar, we now also have massive clumps of rock and dust forming within the disk. This adds a critical new element to the equation that is much more significant on a macroscopic level than in stellar formation: chaos.

The forces of gravity and increasing density of dust particles lead to massive amounts of elastic and inelastic collisions, as rocks ricochet off each other and smash together. Certain clumps of rock inevitably become large and stable enough (and sometimes just lucky enough) to avoid getting broken apart by the impacts. These larger clumps of rock, now having greater gravitational influence due to the added mass, begin sweeping out the local neighborhood as they orbit the protostar, collecting both dust and smaller rocks. Occasionally these boulders will meet other boulders, and interact with each other. This interaction will either result in the two boulders having a near collision, but narrowly missing each other and getting tossed off in opposite directions, or alternatively they will collide, eventually forming an even larger boulder once the dust settles.

This chaotic interaction continues as the boulders grow in size, in some cases, eventually becoming planetesimals, the typically iron-rich cores of future planets. Depending on how much mass a particular planetesimal is able acquire from the surrounding area, they will begin to collect gas from the surrounding area as well, forming an atmosphere. The most massive of planetesimals become gas giants, while the smaller planetesimals become terrestrial planets with defined rocky surfaces. Their composition varies greatly depending on where they formed in the disk, as lighter molecules get blown farther out in the disk by the star's waves of radiation, known in this context as stellar wind. Heavier molecules, which are not so easily blown away, remain closer to the star.

Even at this stage, the nearly fully-formed planets interact with each other and often collide or get tossed towards or away from their parent star, occasionally swapping orbits, until a stable configuration is met. It is this gravitational dance that makes planets like hot Jupiters possible and this is why we find planets of a certain chemical composition much closer or farther away from the parent star (and therefore hotter or cooler) than we would typically expect to find them. In the case of planets, it becomes harder to correlate temperature with interior structure for this reason. In contrast, stars and brown dwarfs are fairly consistent along this relation because of their similar formations.

IIb. Interior Structure

While the surface of our sun and most other main sequence stars is made up of enormous convection cells of hot plasma (called "granules"), this is not the case for most low mass brown dwarfs. While hot high mass brown dwarfs may resemble red dwarfs (both classified as M dwarfs in this case) early in their life cycle, without the driving force of sustained hydrogen

fusion, this semblance disappears as they slowly cool off with time. At some point, the upper atmosphere is cool enough to form cloud layers of heavier elements that one would never find in the upper atmosphere of a main sequence star. These clouds are what set brown dwarfs apart from stars, and are much more akin to what we see upper atmospheres of gas giant planets.

After a brown dwarf has exhausted what little supply of energy it gained from fusion (if it even underwent fusion), it still produces a certain amount of energy in heat through extensive contraction. However, due mostly to convection, heat from the interior is circulated outwards, thus slowly cooling the brown dwarf as it contracts. As the brown dwarf cools, this allows hydrogen to condense with other gasses into layers of molecular clouds. Older, warmer cloud layers slowly descend into the interior as the body contracts, as newer cloud layers form above it.

By looking at the spectra of brown dwarfs, we can see what stage of cooling a brown dwarf currently occupies, based on what cloud layers are detectable in the upper atmosphere (see Lodders et al. 2006). In this manner, brown dwarfs are subdivided into four main classifications from hottest to coolest: "late-M" dwarfs, L dwarfs, T dwarfs, and Y dwarfs. The atmospheres of the first three are compared with that of Jupiter in Figure 3. As mentioned earlier, late-M dwarfs are similar to low mass red dwarfs in both interior structure and outward appearance. At this stage, the brown dwarf is still fusing deuterium, and sometimes even hydrogen, and its upper atmosphere is dominated by carbon monoxide (CO), along with a pronounced cloud layer of corundum (Al_2O_3) and perovskite ($CaTiO_3$), both of which are the characteristic chemical indicators of M dwarfs (Fegley et al. 1996).

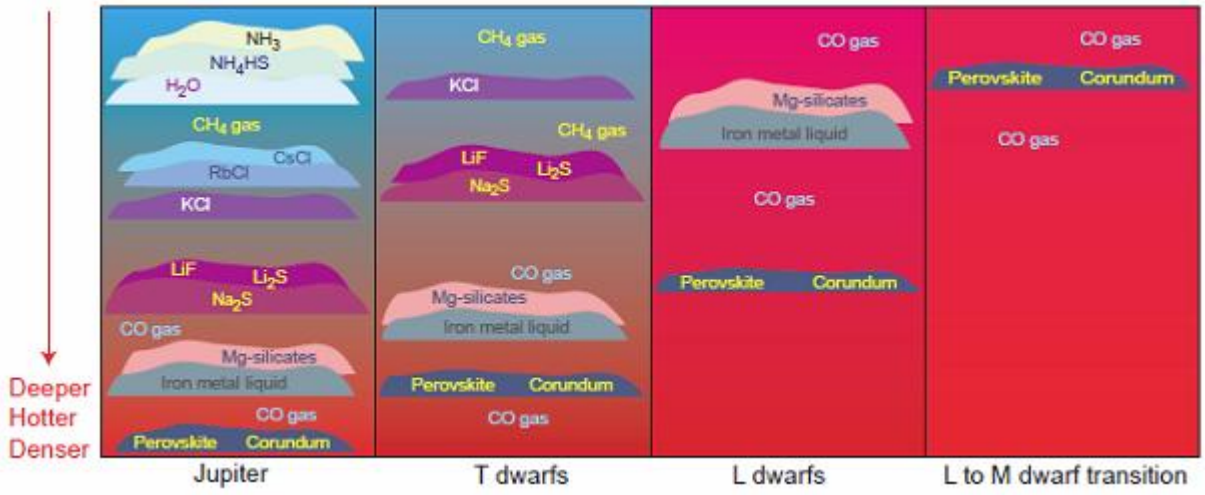

FIG. 3: The upper cloud layers of T, L, and Late-M dwarfs (here labeled "L to M dwarf transition") are juxtaposed with that of Jupiter. Figure is "A cloudy picture" from Lodders 2004.

As it cools, the layer of corundum and perovskite sinks into the interior out of sight, thus becoming an L dwarf. However, it is still warm enough to radiate well on the infrared spectrum, appearing a subdued reddish color on the visible. This glow slowly dims as it continues to cool, and the object becomes less and less bright as more cloud layers form in the upper atmosphere. The first clouds to condense are hot liquidized metals and silicates, primarily iron and magnesium, which occurs at around an effective temperature of 2000K. Once the upper atmosphere sinks below 1500K however, we see a significant transition in chemical composition.

Below this temperature, the CO gas begins to combine with molecular hydrogen (H_2) to produce methane (CH_4) and water vapor (H_2O), which is commonly found in the atmospheres of gas giant planets. As the brown dwarf cools and more CO coverts to CH_4, the upper atmosphere is soon dominated by CH_4. More clouds of molecular condensates form during this transition at around 1000K, including sodium sulfide (Na_2S), lithium fluoride (LiF), lithium sulfide (Li_2S), and later hydrogen chloride (HCl). Brown dwarfs at this stage are referred to as T dwarfs. At this point in its cooling, it has grown much dimmer on the infrared spectrum, and grown more magenta on the visible.

Below 1000K, observation of these objects becomes much more difficult. Y dwarfs, which exist at temperatures below 500K, are much less well understood, though a handful have been discovered within the past couple years. From what we see in the upper atmosphere of Jupiter, we expect ammonia (NH_3) to have a much larger presence. However, ammonia's absorption features are rather similar to that of CH_4 and H_2O, making identification challenging. At this point in its cooling, the brown dwarf is expected to have contracted to roughly the size of Jupiter or smaller. However similar, they still remain fundamentally different objects, which can be identified by a couple key factors.

While the observable condensates in brown dwarfs may vary with age, they are all expected to undergo roughly the same changes, making interior structure easily associated with their current effective temperature, and vice versa. Since they underwent almost identical formation, from very similar environments, it is logical to expect very little deviation from the evolution described above. Planets, in contrast, do not abide by such strict relations. Because of how dynamic planet formation is, the composition of the upper atmosphere can vary from thick cloud layers rich in ammonia and water vapor like Jupiter, or hydrogen and helium, like Saturn, or other molecules containing, similarly to some cold brown dwarfs, sodium and potassium (Brown et al 2001).

While not as easily detectable, we also expect planets to be much richer in elements heavier than He, due to the chemical non-uniformity of the protoplanetary disk. In contrast, we expect nearly all brown dwarfs to possess roughly solar metallicity (logarithmic ratio of H and He abundances to that of other elements). This is especially true for the deeper interiors of planets and brown dwarfs. Planets (including gas giants), which formed from a planetesimal, will typically posses a "rocky" (i.e. metal-based) core. Brown dwarfs, which are primarily H-He based objects, have mostly hydrogen and helium in their cores. However, this goes far beyond what we are able to detect observationally. For this reason, it is more important to focus on hints from the upper atmospheres of these objects.

III. Exoplanet Detection & Obtaining Planet Color

The observation of an object that is several hundred light years away and only a couple thousand kilometers in radius is no small feat, particularly when that object gives off very little light of its own. Perhaps to an astronomer a century ago, this would be a fairly large stretch of the imagination, but with our current level of technology, we have been able to discover not just a handful, but hundreds of extrasolar planets using a variety of methods, often in conjunction with one another. Most of these methods involve indirect detection by observing the parent star of a potential planet. While the parent star often dwarfs its planets in both size and luminosity, any planets that are in orbit will always possess some influence on their parent star's behavior.

Arguably the most easily detectable effect on its parent star is the planet's gravitational influence, which will cause the star to wobble as it rotates. There are two known ways of detecting this type of movement: radial velocity observation and astrometry. Radial velocity observation, or "Doppler spectroscopy," examines how the parent star wobbles to and fro along the line of sight of the observer. Astrometry instead studies how the star bobs from side to side along the plane of the night sky, and was one of the first methods used to try to find extrasolar planets. However, radial velocity observation has proven much more successful, and astrometry is typically only used as an alternative method of confirming previously discovered candidates.

Doppler spectroscopy, as its name suggests, measures the Doppler shift of a star to look for oscillations. If the star is moving towards us, the light coming from the star will appear more blueshifted (with shorter wavelength). Similarly, if it is moving away from us, the light will become more redshifted (with longer wavelength). Since each planet in the system superimposes its own oscillating "semi-amplitude," many stars can have fairly complex fluctuations in their velocity. As shown in De Pater (2001), this semi-amplitude *K* can be related to the mass of the star and several properties of the planet in the following equation:

$$K = \sqrt[3]{\frac{2\pi G}{P_{orb}}}\,\frac{M_P \sin(i)}{(M_P + M_*)^{\frac{2}{3}}}\,\frac{1}{\sqrt{1-e^2}}$$

where G is the gravitational constant, P_{orb} is orbital period, i is the inclination of the orbital plane (the angle between the normal to the plane and our line of sight), e is the eccentricity of the planet's orbit, M_P is the mass of the planet, and M_* is the mass of the star.

By mapping out how the outward velocity of the star oscillates over time, astronomers can model various systems of planets to find the right match. The larger the gravitational influence a particular planet has on the star, the larger the wobble and the easier it is to detect. Consequently, this method is particularly effective at finding massive planets in close orbits like hot Jupiters. The two main drawbacks of this method are: 1) no information about the planet's radius or atmosphere can be found and 2) low mass and far orbiting planets are difficult to detect. Planets with long period orbits can also take decades to confirm. For this reason, astronomers also use a second major technique known as planetary transit detection, which makes up for some of the drawbacks of radial velocity observations.

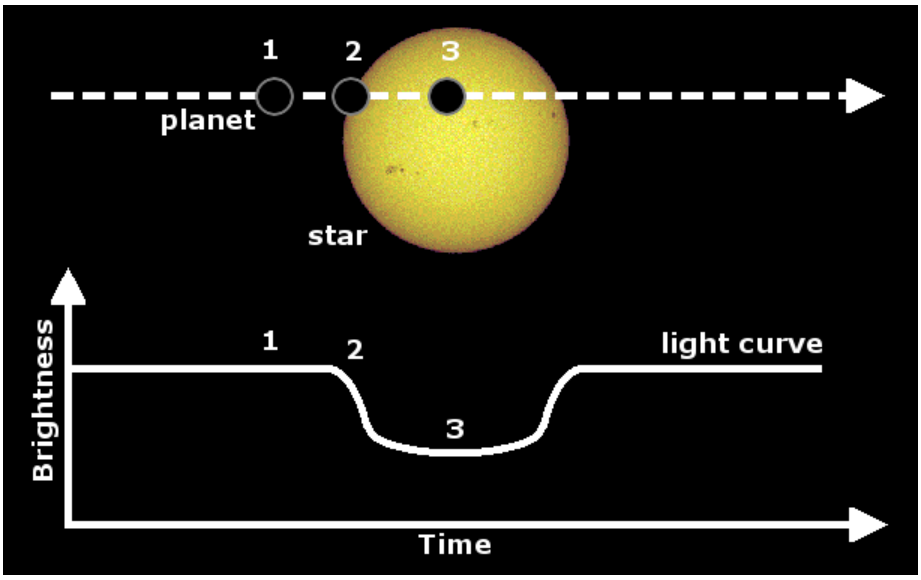

FIG. 4: This figure shows how the brightness of the star dips in magnitude while a planet is in transit across the star's luminous disk. This dip is a rounded square wave. "1" designates the normal brightness of the star before transit, "2" designates the interval of time it takes for the planet to completely enter the stellar disk, and "3" designates the interval of time for the transit to occur, as the planet crosses the stellar disk. Figure based on Image by Centre National d'Etudes Spatiales (CNES).

If a particular exoplanet system is inclined so that the plane of the system is roughly tangential to our line of sight, the orbiting planets will pass between us and their parent star. This type of occurrence is known as a transit. During a transit, the star's luminosity will drop as shown in Figure 4, since it is being partially eclipsed by the passing planet. The star's luminosity will drop again when the planet passes behind the star, as its own reflected light contributes to the star's luminosity shortly before it disappears and reappears on the other side. This is known as a secondary eclipse, or occultance. These drops in luminosity are not instantaneous, and will curve downward for a specific amount of time as the planet enters the parent star's luminous disk. The flux and luminosity also change as the planet orbits around the parent star as shown in Figure 5, between transit and occultation.

From the loss of light during both transits and occultations, one can find the radius of the planet. As shown in Winn et al. (2010):

$$\text{For transits: } \delta_{tra} \approx k^2\left[1 - \frac{I_p(t_{tra})}{I_*}\right] \qquad \text{For occultations: } \delta_{occ} \approx k^2\left[\frac{I_p(t_{occ})}{I_*}\right]$$

where δ is the transit/occultation depth (or the difference in flux), k is the planet-to-star radius ratio (planet radius / star radius), I_p and I_* are the disk-averaged intensities of the planet and star respectively, and t is the transit/occultation time. Combining this information with what was found in radial velocity observations, one can obtain a fairly basic understanding of the planet's size, mass, and orbit. If the planet was first detected via Doppler spectroscopy, one can calculate the probability of a transit by this relation as shown in Charbonnaeu et al. (2006):

$$P_{tr} = 0.0045\ (\frac{1\ \mathrm{AU}}{a})\ (\frac{R_* + R_p}{R_\odot})\ [\frac{1 + e\cos(\frac{\pi}{2} + \varpi)}{1 - e^2}]$$

where a is the semi-major axis, R_*, R_p, and $R_\odot$ are the radii of the parent star, planet, and sun respectively (preferably in solar radii), e is the eccentricity, and ϖ is the longitude of periastron.

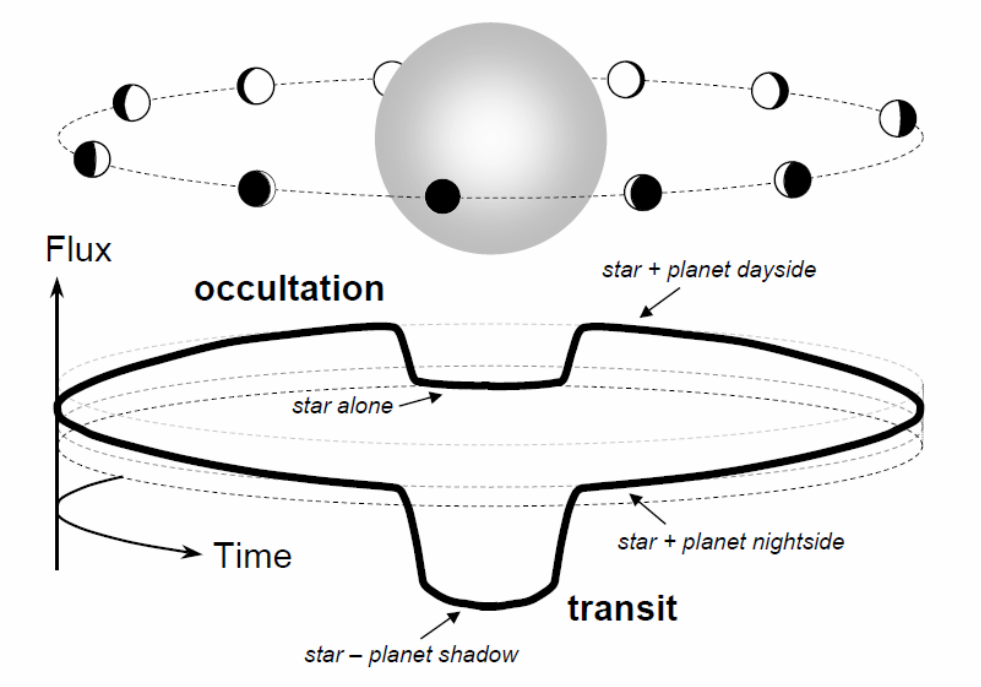

FIG. 5: This figure shows how the flux of the planet-star system varies as the planet orbits around the star. After transit, the flux of the system will slowly increase as the planet reveals more reflected light as it orbits around to the backside of the star, reaching maximum flux just before occultation, before dropping down to a minimum value (in which flux is emanating from the star alone). From the difference between the maximum and minimum fluxes, we can find the flux being received from the planet alone, (Winn et al., 2010).

With the above knowledge in hand, we can obtain a better understanding of the planet by going one step further. We first define the planet-to-star flux ratio (sometimes referred to as the eclipse depth for occultations), r, as:

$$r = \frac{f_0 - f_*}{f_*} = \frac{f_p}{f_*}$$

where f_0 is the flux of the star and planet just before occultation, f_* is the flux of the star alone during occultation, and f_p is the flux of the planet. From this simple relation, we approximate the planet flux in various bandpasses from multiplying the observed flux ratio in a particular bandpass by the calculated flux of the star.

From the planet flux, we can obtain its apparent magnitude in a particular bandpass, and the color between two different bandpasses:

$$m_1 = 2.5 \log_{10} \frac{f_p}{f_v}$$

$$C_{12} = m_1 - m_2 = -2.5 \log_{10} \frac{f_{p1}}{f_{p2}} + 2.5 \log_{10} \frac{f_{v1}}{f_{v2}}$$

where m is the apparent magnitude in a particular bandpass, f_p is the flux of the planet as before, and f_v is the flux of the star, Vega, in that bandpass. In order to make an accurate comparison, these calculations for our purposes were normalized to Vega to match similar color data of brown dwarfs. The uncertainty on the planet flux and color was obtained similarly:

$$\sigma_{f_p} = f_p * (\frac{\sigma_r}{r})$$

$$\sigma_{C_{12}} = \left(\frac{2.5}{\ln 10}\right) \sqrt{(\frac{\sigma_{f_{p1}}}{f_{p1}})^2 + (\frac{\sigma_{f_{p2}}}{f_{p2}})^2}$$

where σ_r is the uncertainty on the planet-to-star flux ratio, σ_{f_p} is the uncertainty on the planet flux, and σ_C is the uncertainty on the color. The uncertainties on Vega's fluxes are negligible and were not included.

Lastly, since the temperatures of the planets and brown dwarfs are not directly observed, we calculated them from known parameters. For the brown dwarfs, we used a spectral type-effective temperature relationship modeled by Stephens et al. (2009) using the following equation:

$$T_{eff} = 2265.9 + 347.82 t_{IR} - 60.588 t_{IR}^2 + 3.151 t_{IR}^3 - 0.060481 t_{IR}^4 + 0.00024506 t_{IR}^5$$

where t_{IR} corresponds to the spectral type where M0 through M9 are $t_{IR} = 0,1,2, \ldots 8,9$, L0 through L9 are $t_{IR} = 10,11,12, \ldots 18,19$, T0 through T9 are $t_{IR} = 20,21,22, \ldots 28,29$, and Y0 through Y9 are $t_{IR} = 30,31,32, \ldots 38,39$. The scattering in this fit is about 100K. For planets, the effective temperature (often referred to as equilibrium temperature in this context) is calculated from the parent star's as well as a number of other parameters in this following equation, as shown in Seager et al. (2005):

$$T_{eq} = T_{eff} * \sqrt{\frac{R_{star}}{2 * a}}$$

where T_{eff} in this case is the parent star's effective temperature, R_{star} is the stellar radius, and a is the semi-major axis. It should be noted that R_{star} and a were converted into units of centimeters from solar radii and AU respectively. Also, the traditional form of this equation includes a factor of *(1-A)* multiplied to the temperature where *A* is the Bond albedo or reflectivity of the planet. We have calculated the effective temperature assuming that the Bond albedo is zero, i.e. that the planet can be approximated as a blackbody. The uncertainty on this temperature is as follows:

$$\sigma_{T_{eq}} = T_{eq} * \sqrt{(\frac{\sigma_{T_{eff}}}{T_{eff}})^2 + (\frac{\sigma_{R_{star}}}{4 * R_{star}})^2}$$

where $\sigma_{T_{eff}}$ and $\sigma_{R_{star}}$ are the uncertainties on the parent star's effective temperature and radius, respectively.

IV. Constructing Profiles for Gas Giant Planets & Brown Dwarfs

By comparing the trends in color and temperature among brown dwarfs and planets, we expect to find a number of noticeable differences that arise from their dissimilar formations and interiors. To confirm this, we put together a catalog of a wide variety of brown dwarfs and planet-star systems that had their fluxes measured in the 3.6, 4.5, 5.8, and 8.0 micron bands by the Infrared Array Camera (IRAC) on the *Spitzer Space Telescope*.

The data regarding the brown dwarfs was obtained from two major sources: a recent catalog of *Wide-Field Infrared Survey Explorer* (*WISE)* and *Spitzer* data compiled by Kirkpatrick et al. (2011), and a second catalog of *Spitzer* data compiled by Leggett et al. (2010), which included data from Burgasser et al. (2008), Burningham et al. (2008), Luhman et al. (2007), Patten et al. (2006), and Warren et al. (2007). We also added a recent low-temperature brown dwarf from Luhman et al. (2012). For planet data, we used a catalog of large gas giant planets compiled by Seager & Deming (2010, priv. comm. 2011). Our overall data currently includes 30 planets and 210 brown dwarfs. Vega's flux data was also obtained from Patten et al. (2006). To further investigate this dissimilarity, we also modeled a number of planet and brown dwarf atmospheres based on a format presented by Fortney et al. (2008). We were then able to obtain a pressure-temperature profile that compared two known planets to a number of brown dwarf models we created.

We used the remaining data to construct a number of profiles including a radius-color-temperature "diversity profile" for both the planet data and the brown dwarf data and a number of color temperature profiles displaying both data sets. We constructed the former to illustrate the diverse and complex nature of planets in contrast to the evenly assorted brown dwarfs. We plotted both data sets in the color-temperature profile to contrast the clear trend seen among brown dwarfs to the large scattering of planets. We used two main IDL procedures to accomplish this.

The first procedure we created was one to calculate the individual star and planet color (and the associated uncertainties). To do this, we read in two main data files regarding an individual planetary system. The first, as shown in Tables 1 & 2 (see Section VII), contained the planet-to-star flux ratios for two to four different IRAC bandpasses, their uncertainties, and a number of other parameters needed, including the parent star's T_{eff} and radius, as well as the planet's own radius and semi-major axis, as shown in Table 3. The second data file read in table of wavelength and flux values generated from a stellar model by Hauschildt et al. (1999), using values for T_{eff} and surface gravity that match the parent star's.

In order to obtain an accurate stellar flux for each bandpass, we had to interpolate our stellar flux data onto the four IRAC bandpasses we used. To do this, we read in a wavelength-transmission table for each IRAC bandpass, converted this into a frequency table and then interpolated our stellar flux data onto these four IRAC bandpasses. We then integrated the now interpolated stellar flux times the transmission over a particular frequency grid, and then divided by the integral of the transmission over that frequency grid, as shown in the following equation:

$$f_* = \frac{\int f(\nu)\,\tau(\nu)\,d\nu}{\int \tau(\nu)\,d\nu}$$

Where $f(\nu)$ is the interpolated stellar model flux (in terms of frequency, ν), $\tau(\nu)$ is the transmission coefficient, and f_* is the single value for the parent star's flux that we obtain for a particular wavelength. This is repeated for each of the four IRAC bandpasses, finally giving us the stellar flux at each bandpass. With this in hand, it was a simple matter of obtaining the planet and parent star color using the methods described in Section III. This procedure was repeated for each planet in our data set until we obtained all the colors shown in Tables 4A, 4B, and 5.

The second procedure reads in the planet data given in Tables 1-4B and the brown dwarf data given in Table 6, and a data file containing the color-temperature profile of a blackbody. Next, it computes the T_{eff} for each planet and brown dwarf as shown in Section III. With these all brought together, it then plots all of the data on a color versus T_{eff} profile, including the uncertainties on the color for each object. The uncertainties on the T_{eff} for each individual object are not plotted to reduce clutter. Instead, we calculated the average uncertainty for the temperatures in planet data set and the brown dwarf data set, and then plotted these on the side. We repeated this color-temperature profile for each combination of magnitudes. We also used this data to create our "diversity profile" for both the planet data set and the brown dwarf data set on a radius-temperature profile. In these two profiles, each object is represented by a circle that's size and color is scaled relative to each object's color and radius.

V. Exhibiting Differing Trends among Planets & Brown Dwarfs

As described in Section II, there are many different factors that contribute to the trends we expect to see among planets and brown dwarfs. Before even taking planet diversity into consideration, we would expect these two types of objects to show very different types of trends because of how heat is generated and transferred inside their interiors. The depths at which we observe their effective temperature differ greatly between that of planets and brown dwarfs due to temperature inversion, as shown in Figure 6. Here, we have plotted two planet models and three brown dwarf models at varying temperatures. The dots on each line mark the effective temperature of that object, and what the pressure of the atmosphere is at that depth. Since the temperature inversion raises the relative altitude at which we observe the object's flux, we are observing a different region of the atmosphere than that of an identical object without temperature inversion.

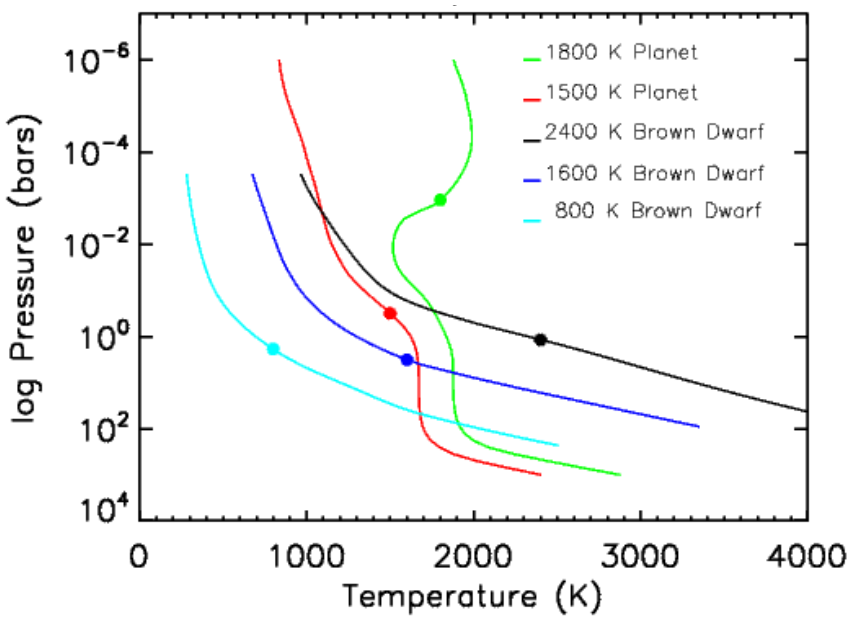

FIG. 6: Three brown dwarf and two planet models are plotted along a pressure-temperature profile. All models are calculated in radiative-convective equilibrium. The brown dwarf models are heated from their interior, while the planet models are heated from their parent star. The three brown dwarf models are run with a surface gravity of 1000 m/s^2 and at effective temperatures of 800K, 1600K, and 2400K. The two planet models are based on HD189733b and HD209458b. HD189733b and HD209458b in these models have effective temperatures of 1500K and 1800K respectively (which are based on wavelength-flux simulations, instead of the method shown in Section III). The effective temperature and the pressure at the depth it's observed are marked by dots. All profiles are based on a model presented by Fortney et al. (2008).

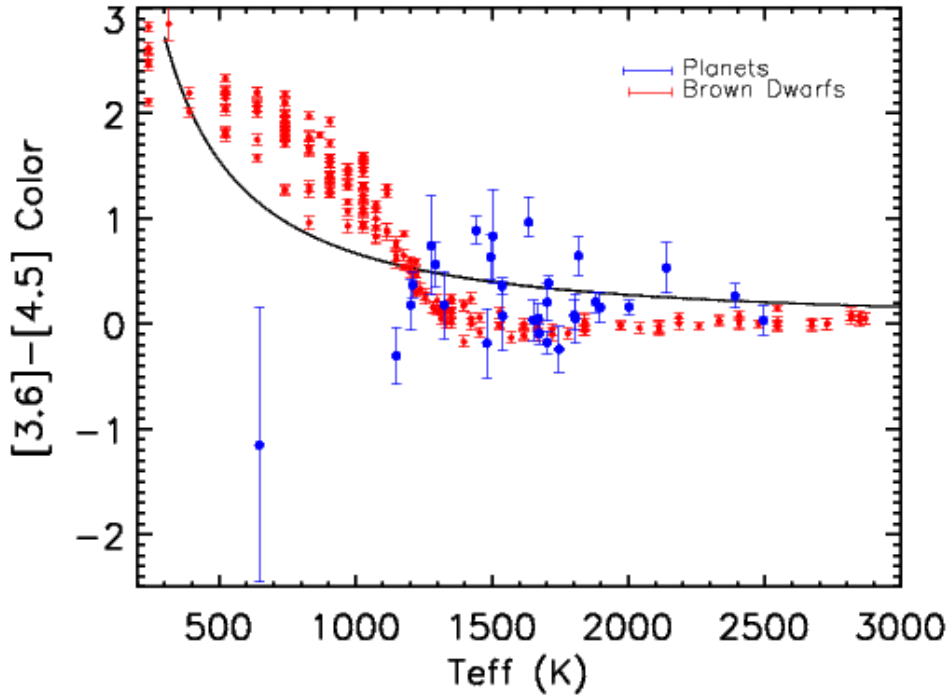

FIG. 7: [3.6μm]-[4.5μm] color versus effective temperature in K for known brown dwarfs (in red) and planets (in blue), as well as for a uniform blackbody model (in black). Uncertainties in color for individual objects are shown, average uncertainties in temperature are shown on upper right. Plot is based on data shown in Table 4A & 7A.

The diversity of chemical abundances that one would find the upper cloud layers of gas giant planets would consequently lead to a lot of diverse absorption features in the colors of the planets. Depending what types of temperature inversions those chemicals are causing, the colors that would be observed from the flux of the planet could have passed through any number of depths and cloud layers before being reflected to cause those absorption features. This large variance of color is exhibited in stark contrast to the consistent color-temperature relationship of brown dwarfs in Figure 7. Here we have plotted the [3.6μm]-[4.5μm] color (the two wavelengths with the most flux data) versus the effective temperature of our entire planet and brown dwarf data sets, as well as a blackbody line for means of comparison. Color-temperature profiles for other used flux bands in this study are shown in Figures 10-14 (see Section VIII).

To further exhibit diversity, radius-color-temperature "diversity plots" are shown in Figures 8 for planets and Figure 9 for brown dwarfs. All colors in these two figures are relative infrared [3.6μm]-[4.5μm] colors on a blue-to-red scale. While the brown dwarfs follow a consistent relationship between radius and temperature and color as they do in Figure 7, the planets are much more scattered with no distinct relationship between color, radius, and temperature. However, on average, colder planets seem to be smaller and exhibit "bluer" color. For the sake of clarity, not all brown dwarf data points are shown. Brown Dwarf radius is estimated using a model created by Baraffe et al. (2003) based on calculated T_{eff}, and assuming all brown dwarfs are between 0.5 to 10Gyr old. Diversity plots using colors for other IRAC band combinations are shown in Figures 15-18 (see Section VIII).

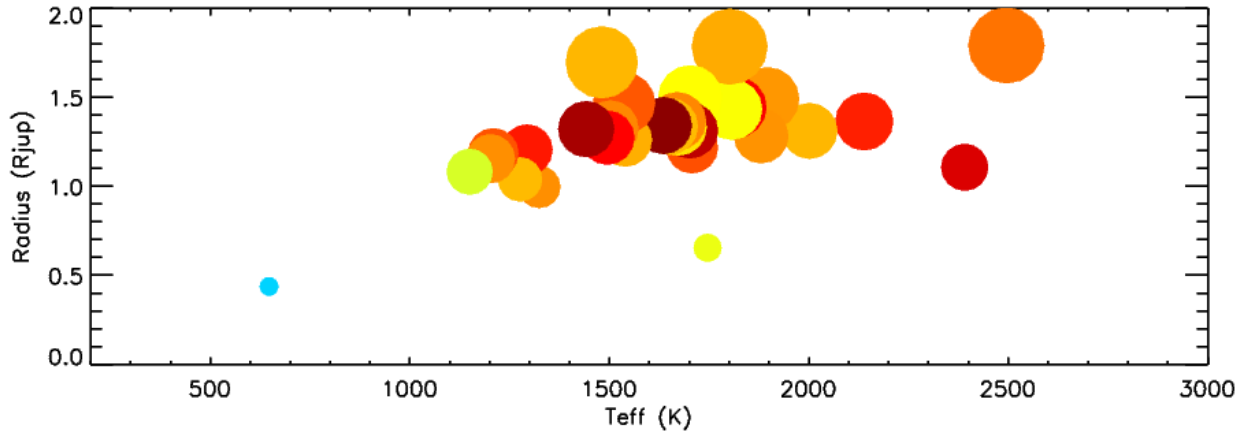

FIG. 8: Diversity plot for 30 planets. Planets are colored on a blue-to-red scale based on their [3.6μm]-[4.5μm] color and scaled based on their radius. Objects with more positive color on this case are redder, and those with more negative color are bluer (and would appear so to an observer viewing them on these infrared wavelengths). Plot is based on data in Tables 2 & 4A.

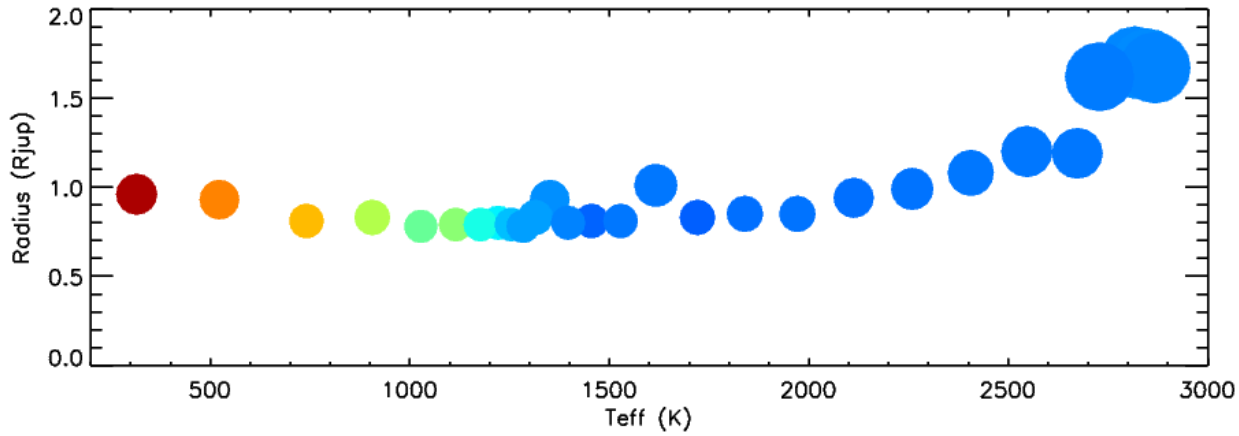

FIG. 9: Diversity plot for 28 brown dwarfs. These are also colored on a blue-to-red scale based on their [3.6μm]-[4.5μm] color and scaled based on their estimated radius, which is based on a brown dwarf model created by Baraffe et al. (2003). Plot is based on this model as well as data shown in Table 6 & 7A. While the radius scale is the same as Figure 8, the color scale is contracted since brown dwarfs rarely have substantially negative [3.6μm]-[4.5μm] color.

VI. Conclusions

Figures 7-9 confirm our expectations on the distribution of planets and brown dwarfs across a color-effective temperature relationship. The two most immediately noticeable things in these figures are 1) the consistent relationship among all brown dwarfs and 2) the general scattering of planets in contrast. Although the uncertainties on the planets are larger than that of the brown dwarfs, the scattering is still large enough to still be significant. This also confirms that all brown dwarfs follow roughly the same chemical evolution in their upper atmosphere as they cool and contract.

As shown in Figure 7, above 1500K, most brown dwarfs have a [3.6μm]-[4.5μm] color of around zero or slightly less. Above this temperature, as described in Section II, the atmosphere is mostly dominated by CO, a strong absorber on the 4.5μm IRAC band. Below 1500K, this CO begins to convert into CH_4, which is a particularly strong absorber on the 3.6μm IRAC band. This chemical reaction leads to the upward trend we see in the figure; as the CH_4/CO ratio increases, the [3.6μm]-[4.5μm] color becomes more positive, bending above the blackbody line. The slight scattering in the brown dwarfs below 1200K is due to an increase in uncertainty in the spectral type and therefore the T_{eff}. The upward trend begins to level out below 1000K when CH_4 dominates the upper atmosphere and most of the observable CO supply has been exhausted or sunk deeper into the interior out of sight. As the brown dwarfs cool off further, the color continues to increase alongside the black body line. No data is yet available below 200K.

The influence of CH_4 and CO is also evident in Figures 10-14. Figures 10 and 14, which shows the [4.5μm-5.8μm] and [4.5μm-8.0μm] color versus T_{eff} respectively, shows decreasing color in brown dwarfs below 1500K as to be expected, due to the decreasing portions of CO and CO_2 below that temperature. On wavelength bands without such strong absorption features, those trends disappear, as shown in Figure 11, which shows [5.8μm-8.0μm] color versus T_{eff}. In this figure, brown dwarfs and planets alike follow the blackbody line much more closely. Adding in the 3.6μm band in again in Figures 12 and 13, which show [3.6μm-5.8μm] and

[3.6μm-8.0μm] color versus T_{eff} respectively, the trends due to CH_4 absorption return as expected. Interestingly, the planets show a rather different assortment between Figures 12 and 13, in contrast to the brown dwarfs, which are arranged in more or less the same trend. This is also evident in the other color-temperature profiles.

In all Figures 7 & 10-14, planets are scattered far above and below the blackbody line. The coldest planet in this data set, GJ-436b, can be seen on the lower left hand of Figure 7. It's divergence from the main grouping of gas giants may suggest either a downward trend with temperature or that it is very chemically different from the other planets in this data set. It's extremely negative color indicates an extreme absence of CH_4 in addition to an abundance of chemical(s) that are strong absorbers on the 4.5μm band, such as CO and CO_2. This is consistent with previous studies on the planet (Stevenson et al. 2010, & Line et al. 2011), and more data of planets below 1200K should shed some light on this peculiarity. Interestingly, in the current set of data, no planets exist above the blackbody line below 1250K. If this remains true as more data is collected below this temperature, this could indicate that the absence of methane may not be that uncommon on this range of temperatures. As shown in Figure 8, there also appears to be no correlation between radius and color among planets as there is among brown dwarfs as shown in Figure 9. Since brown dwarfs follow nearly identical chemical evolutions, they will contract and cool along the same relationship. Planets, in contrast, are much more chemically exotic.

As described in Section II, the two most significant factors in this are their striking diversity from their formation, and their absorption of light from their parent star, leading to the temperature inversions shown in Figure 6. Their chemical composition will differ dramatically, depending on where they formed in their parent star's protoplanetary disk. Their effective temperature is dependent on the total flux that they receive from their parent star, and what type of cloud layers in their upper atmosphere would absorb that light. The relationship between these two is entirely dependent on what types of gravitational interactions these planets went through during formation and led them to their current orbital distance and the temperature of the regions of their atmosphere that we are observing, and whether these regions are subject to temperature inversion. Putting all of these factors together is only the icing on the cake in our understanding of the complexity and diversity of these objects together. So it is no small wonder that any patterns, if there are any, are difficult to discern among the gas giant planet color.

Once detailed spectroscopy of these atmospheres is possible, perhaps once the *James Webb Space Telescope (JWST)* is finally launched and in operation, we will able to gain a much better means of understanding and classifying these objects. However, until we reach that point, which may not be for another decade or more, it is important to uncover as much information as we can about these objects through photometry, as this will provide us a guide of what chemicals to look for when accurate spectroscopy of low temperature gas giants, and planets overall, becomes feasible. There remains a lot for us to learn about these objects in the coming years, but with the abundance of planets being discovered monthly and the increasing number of planets with photometric data available, the future of this field is incredibly promising, and I for one can't wait to see what we find.

VII. Appendix of Tables

TABLE 1
Planet-To-Star Flux Ratios

Name	$r_{3.6\mu m}$	σ_{r-}	σ_{r+}	$r_{4.5\mu m}$	σ_{r-}	σ_{r+}	$r_{5.8\mu m}$	σ_{r-}	σ_{r+}	$r_{8.0\mu m}$	σ_{r-}	σ_{r+}	Ref. #
CoRoT-1	0.415	0.042	0.042	0.482	0.042	0.042							1
CoRoT-2	0.355	0.020	0.020	0.500	0.020	0.020				0.409	0.080	0.080	1
GJ-436	0.030	0.020	0.020	0.010	0.010	0.010	0.033	0.014	0.014	0.054	0.008	0.008	2, 3
HAT-P-1	0.080	0.008	0.008	0.135	0.022	0.022	0.203	0.031	0.031	0.238	0.040	0.040	4
HAT-P-5	0.116	0.024	0.024	0.125	0.028	0.028							5
HAT-P-6	0.117	0.008	0.008	0.106	0.006	0.006							6
HAT-P-7	0.098	0.017	0.017	0.159	0.022	0.022	0.245	0.031	0.031	0.225	0.052	0.052	7
HAT-P-8	0.131	0.009	0.009	0.111	0.008	0.008							6
HD149026	0.040	0.003	0.003	0.032	0.006	0.006	0.043	0.009	0.009	0.050	0.006	0.006	8
HD189733	0.147	0.004	0.004	0.179	0.040	0.040	0.310	0.034	0.034	0.365	0.011	0.011	9, 10
HD209458	0.094	0.009	0.009	0.213	0.015	0.015	0.301	0.043	0.043	0.230	0.013	0.013	11, 10
Kepler-5	0.137	0.020	0.020	0.116	0.031	0.031							12
Kepler-6	0.250	0.030	0.030	0.310	0.035	0.035							12
Kepler-12	0.103	0.017	0.017	0.107	0.015	0.015							13
Kepler-17	0.069	0.027	0.027	0.151	0.019	0.019							14
TrES-1	0.085	0.013	0.013	0.066	0.013	0.013				0.225	0.036	0.036	10, 15
TrES-2	0.127	0.021	0.021	0.230	0.024	0.024	0.199	0.054	0.054	0.359	0.060	0.060	16
TrES-3	0.356	0.035	0.035	0.372	0.054	0.054	0.449	0.097	0.097	0.475	0.046	0.046	17
TrES-4	0.137	0.011	0.011	0.148	0.016	0.016	0.261	0.059	0.059	0.318	0.044	0.044	18
WASP-1	0.117	0.016	0.016	0.212	0.021	0.021	0.282	0.060	0.060	0.470	0.046	0.046	19
WASP-2	0.380	0.040	0.040	0.390	0.030	0.030	0.629	0.052	0.052	0.636	0.067	0.067	19
WASP-4	0.187	0.007	0.007	0.224	0.018	0.018							20
WASP-12	0.300	0.020	0.020	0.380	0.030	0.030	0.410	0.020	0.020	0.430	0.030	0.030	21, 22
WASP-14	0.483	0.020	0.013	0.572	0.030	0.030	0.588	0.049	0.049	0.594	0.105	0.105	23
WASP-18	0.083	0.035	0.035	0.169	0.017	0.017	0.192	0.077	0.077	0.285	0.059	0.059	24
WASP-19	0.320	0.031	0.031	0.343	0.027	0.027							25
XO-1	0.086	0.007	0.007	0.122	0.009	0.009	0.261	0.031	0.031	0.210	0.029	0.029	26
XO-2	0.081	0.017	0.017	0.098	0.020	0.020	0.167	0.036	0.036	0.133	0.049	0.049	27
XO-3	0.101	0.004	0.004	0.143	0.006	0.006	0.134	0.049	0.049	0.150	0.036	0.036	28
XO-4	0.056	0.006	0.012	0.135	0.009	0.009							6

REFERENCES. — (1) Deming et al. (2011); (2) Beaulieu et al. (2011); (3) Stevenson et al. (2010); (4) Todorov et al. (2010); (5) Désert et al., in prep.; (6) Todorov et al. (2012); (7) Christiansen et al. (2010); (8) Stevenson et al. (2011); (9) Charbonneau et al. (2008); (10) Knutson et al., in prep.; (11) Knutson et al. (2008); (12) Désert et al. (2011a); (13) Fortney et al. (2011); (14) Désert et al. (2011b); (15) Charbonneau et al. (2005); (16) O'Donovan et al. (2010); (17) Fressin et al. (2010); (18) Knutson et al. (2009); (19) Wheatley et al. (2010); (20) Beerer et al. (2011); (21) Cowan et al. (2012); (22) Madhusudhan et al. (2011); (23) Blecic et al., in prep.; (24) Nymeyer et al. (2011); (25) Anderson et al., in prep.; (26) Machalek et al. (2008); (27) Machalek et al. (2009); (28) Machalek et al. (2010).

TABLE 2
Planet Mass, Radius, Orbital Period, and Semi-Major Axis

Name	M_p (M_{jup})	σ_{Mp}	R_p (R_{jup})	σ_{Rp-}	σ_{Rp+}	P_{orb} (days)	a (AU)	Ref. #
COROT-1b	1.03	0.12	1.49	0.08	0.08	1.508956	0.0254	1
COROT-2b	3.31	0.16	1.465	0.029	0.029	1.742996	0.0281	2
GJ-436b	0.071	0.006	0.437	0.035	0.035	2.643904	0.02872	3
HAT-P-1b	0.53	0.04	1.203	0.051	0.051	4.46529	0.0553	4
HAT-P-5b	1.06	0.11	1.26	0.05	0.05	2.788491	0.04075	5
HAT-P-6b	1.057	0.119	1.33	0.061	0.061	3.852985	0.05235	6
HAT-P-7b	1.776	0.006	1.363	0.087	0.195	2.20473	0.0377	7
HAT-P-8b	1.52	0.17	1.5	0.06	0.08	3.07632	0.0487	8
HD149026b	0.36	0.03	0.654	0.045	0.06	2.875889	0.04313	9, 10, 11
HD189733b	1.15	0.04	1.154	0.017	0.017	2.218581	0.03099	9, 11, 12
HD209458b	0.657	0.006	1.32	0.025	0.025	3.524749	0.04707	9, 13
Kepler-5b	2.114	0.059	1.431	0.052	0.052	3.54846	0.05064	14
Kepler-6b	0.669	0.03	1.323	0.029	0.029	3.234723	0.04567	15
Kepler-12b	0.431	0.041	1.695	0.032	0.028	4.4379637	0.0556	16
Kepler-17b	2.45	0.114	1.312	0.018	0.018	1.485711	0.02591	17
TrES-1	0.76	0.05	1.081	0.029	0.029	3.030074	0.0393	9, 18, 19
TrES-2	1.198	0.053	1.272	0.041	0.041	2.470613	0.03556	9, 20, 21, 22
TrES-3	1.91	0.08	1.336	0.034	0.034	1.306186	0.0226	9, 22, 23
TrES-4	0.925	0.08	1.783	0.09	0.09	3.553945	0.05091	24
WASP-1b	0.867	0.073	1.443	0.039	0.039	2.519961	0.0382	9, 25, 26
WASP-2b	0.88	0.07	1.038	0.05	0.05	2.152226	0.03138	9, 25, 20
WASP-4b	1.237	0.064	1.365	0.021	0.021	1.338232	0.023	27
WASP-12b	1.41	0.09	1.79	0.09	0.09	1.091423	0.0229	24
WASP-14b	7.341	0.502	1.281	0.075	0.082	2.2437661	0.036	28, 29
WASP-18b	10.3	0.69	1.106	0.072	0.072	0.941453	0.02026	30, 31
WASP-19b	1.15	0.08	1.31	0.06	0.06	0.78884	0.0165	32
XO-1b	0.9	0.07	1.184	0.018	0.028	3.941534	0.0488	33, 34, 35
XO-2b	0.565	0.054	0.996	0.018	0.029	2.615864	0.0369	36, 37
XO-3b	11.79	0.59	1.217	0.073	0.073	3.191524	0.0454	38
XO-4b	1.72	0.2	1.34	0.05	0.05	4.12502	0.0555	39, 40

REFERENCES. — (1) Barge et al. (2008); (2) Alonso et al. (2008); (3) Torres (2007); (4) Johnson et al. (2008); (5) Bakos et al. (2007b); (6) Noyes et al. (2008); (7) Pál (2012); (8) Moutou et al. (2011); (9) Southworth (2010); (10) Stevenson et al. (2011); (11) Triaud et al. (2010); (12) Torres et al. (2008); (13) Southworth (2008); (14) Borucki et al. (2010); (15) Dunham et al. (2010); (16) Fortney et al. (2011); (17) Désert et al. (2011b); (18) Charbonneau et al. (2005); (19) Raetz et al. (2009); (20) Daemegn et al. (2009); (21) Schröter et al. (2012); (22) Christiansen et al. (2011); (23) O'Donovan et al. (2007); (24) Chan et al. (2011); (25) Albrecht et al. (2011); (26) Cameron et al. (2007a); (27) Sanchis-Ojeda et al. (2011); (28) Blecic et al., in prep.; (29) Joshi et al. (2008); (30) Southworth et al. (2009); (31) Nymeyer et al. (2011); (32) Hellier et al. (2011); (33) McCullough et al. (2006); (34) Holman et al. (2006); (35) Cáceres et al. (2009); (36) Narita et al. (2011); (37) Burke et al. (2007); (38) Winn et al. (2008); (39) McCullough et al. (2008); (40) Todorov et al. (2012).

TABLE 3
Parent Star Mass, Radius, Effective Temperature, and Metallicity

Name	M_{star} (M_{sun})	σ_{Mstar}	R_{star} (R_{sun})	σ_{Rstar}	T_{eff} (K)	σ_{Teff}	[Fe/H]	$\sigma_{[Fe/H]}$	Ref. #
COROT-1	0.95	0.15	1.11	0.05	5950	150	-0.3	0.25	1
COROT-2	0.97	0.06	0.902	0.018	5625	120	0	0.2	2, 3
GJ-436	0.44	0.04	0.505	0.025	3200	200	-0.03	0.2	4, 5
HAT-P-1	1.12	0.09	1.115	0.043	5975	45	0.13	0.02	6, 7
HAT-P-5	1.16	0.06	1.17	0.05	5960	100	0.24	0.15	8, 9
HAT-P-6	1.29	0.06	1.46	0.06	6570	80	-0.13	0.08	10
HAT-P-7	1.47	0.07	1.84	0.17	6350	80	0.26	0.08	11
HAT-P-8	1.28	0.04	1.58	0.07	6200	80	0.01	0.08	12
HD149026	1.3	0.06	1.497	0.069	6147	50	0.36	0.05	13, 14
HD189733	0.82	0.03	0.755	0.011	5050	50	-0.03	0.04	15, 16, 17
HD209458	1.101	0.064	1.125	0.022	6117	26	0.02	0.03	18, 19, 20, 21
Kepler-5	1.166	0.0525	1.483	0.027	5947	100	0.07	0.04	22
Kepler-6	1.061	0.067	1.019	0.033	5630	100	0.3	0.1	23
Kepler-12	1.374	0.059	1.793	0.062	6297	60	0.04	0.06	24
Kepler-17	1.209	0.044	1.391	0.034	5647	44	0.34	0.04	25
TrES-1	0.89	0.035	0.811	0.02	5250	75	-0.02	0.06	26
TrES-2	0.98	0.062	0.999	0.033	5850	50	-0.15	0.1	27, 28
TrES-3	0.93	0.04	0.83	0.02	5650	175	-0.19	0.08	29, 30
TrES-4	1.4	0.1	1.849	0.09	6200	75	0.14	0.09	31
WASP-1	1.15	0.09	1.453	0.032	6110	245	0.23	0.08	32, 33, 34
WASP-2	1.35	0.14	1.57	0.07	6250	150	0.25	0.1	32, 33, 35
WASP-4	1.211	0.1245	1.306	0.0695	6475	100	0	0.2	35, 36
WASP-12	1.25	0.13	1.216	0.067	6400	100	0	0.09	31
WASP-14	0.96	0.1	0.94	0.04	5500	100	0.02	0.09	37, 38
WASP-18	0.79	0.09	0.813	0.032	5200	200	0	0.2	35, 39, 40
WASP-19	0.925	0.04	0.912	0.013	5500	150	-0.03	0.09	41, 42
XO-1	1	0.03	0.928	0.033	5750	13	0.015	0.03	43, 44
XO-2	0.971	0.034	0.976	0.032	5340	32	0.45	0.02	45
XO-3	1.213	0.066	1.377	0.083	6429	100	-0.18	0.08	46
XO-4	1.32	0.02	1.56	0.05	6397	70	-0.04	0.03	47

REFERENCES. — (1) Barge et al. (2008); (2) Alonso et al. (2008); (3) Bouchy et al. (2008); (4) Torres (2007); (5) Bean et al. (2006); (6) Johnson et al. (2008); (7) Bakos et al. (2007a); (8) Southworth et al. (2012); (9) Bakos et al. (2007b); (10) Noyes et al. (2008); (11) Pál et al. (2008); (12) Latham et al. (2009); (13) Sato et al. (2005); (14) Nutzman et al. (2009); (15) Nordström et al. (2004); (16) Baines et al. (2008); (17) Belle (2008); (18) Southworth (2010); (19) Brown et al. (2001); (20) Schuler et al. (2011); (21) Santos et al. (2003); (22) Borucki et al. (2010); (23) Dunham et al. (2010); (24) Fortney et al. (2011); (25) Bonomo et al. (2012); (26) Alonso et al. (2004); (27) Daemgen et al. (2009); (28) Sozzetti et al. (2007a); (29) Sozzetti et al. (2007b); (30) O'Donovan et al. (2007); (31) Chan et al. (2011); (32) Cameron et al. (2007a); (33) Cameron et al. (2007b); (34) Stempels et al. (2007); (35) Triaud et al. (2010); (36) Wilson et al. (2008); (37) Blecic et al., in prep.; (38) Joshi et al. (2008); (39) Southworth et al. (2009); (40) Hellier et al. (2009); (41) Hellier et al. (2011); (42) Hebb et al. (2010); (43) McCullough et al. (2006); (44) Holman et al. (2006); (45) Burke et al. (2007); (46) Winn et al. (2008); (47) McCullough et al. (2008).

TABLE 4A
Planet Temperature and Colors

Name	T_{eff} (K)	σ_T (K)	$C_{[3.6-4.5\mu m]}$	σ_{c-}	σ_{c+}	$C_{[4.5-5.8\mu m]}$	σ_{c-}	σ_{c+}	$C_{[5.8-8.0\mu m]}$	σ_{c-}	σ_{c+}
COROT-1b	1896	64	0.157	0.145	0.145						
COROT-2b	1537	36	0.358	0.075	0.075						
GJ-436b	647	43	-1.150	1.305	1.305	1.348	1.179	1.179	0.610	0.488	0.488
HAT-P-1b	1294	27	0.563	0.208	0.208	0.447	0.242	0.242	0.195	0.247	0.247
HAT-P-5b	1540	42	0.075	0.331	0.331						
HAT-P-6b	1673	40	-0.094	0.096	0.096						
HAT-P-7b	2139	102	0.534	0.241	0.241	0.469	0.204	0.204	-0.080	0.286	0.286
HAT-P-8b	1703	44	-0.176	0.105	0.105						
HD149026b	1746	43	-0.241	0.219	0.219	0.323	0.305	0.305	0.181	0.262	0.262
HD189733b	1202	15	0.180	0.244	0.244	0.609	0.270	0.270	0.225	0.124	0.124
HD209458b	1442	15	0.889	0.129	0.129	0.378	0.173	0.173	-0.276	0.167	0.167
Kepler-5b	1807	36	-0.186	0.331	0.331						
Kepler-6b	1503	22	0.203	0.179	0.179						
Kepler-12b	1481	28	0.048	0.235	0.235						
Kepler-17b	1702	41	0.834	0.446	0.446						
TrES-1b	1150	22	-0.302	0.271	0.271						
TrES-2b	1495	28	0.635	0.212	0.212	-0.152	0.316	0.316	0.667	0.346	0.346
TrES-3b	1651	55	0.037	0.190	0.190	0.210	0.283	0.283	0.090	0.257	0.257
TrES-4b	1801	49	0.084	0.146	0.146	0.619	0.272	0.272	0.233	0.288	0.288
WASP-1b	1817	76	0.646	0.183	0.183	0.313	0.255	0.255	0.573	0.254	0.254
WASP-2b	1276	55	0.033	0.142	0.142	0.150	0.449	0.449	0.474	0.490	0.490
WASP-4b	1670	47	0.207	0.096	0.096						
WASP-12b	2495	82	0.266	0.112	0.112	0.520	0.123	0.123	0.027	0.145	0.145
WASP-14b	1880	58	0.162	0.073	0.064						
WASP-18b	2391	76	0.743	0.471	0.471	0.082	0.101	0.101	0.063	0.092	0.092
WASP-19b	2001	56	0.054	0.136	0.136	0.038	0.107	0.107	0.050	0.212	0.212
XO-1b	1209	22	0.370	0.119	0.119	0.832	0.152	0.152	-0.208	0.198	0.198
XO-2b	1324	23	0.179	0.318	0.318	0.588	0.322	0.322	-0.202	0.463	0.463
XO-3b	1707	58	0.388	0.063	0.063	-0.072	0.400	0.400	0.133	0.475	0.475
XO-4b	1635	32	0.965	0.137	0.244						

TABLE 4B
Other Planet Colors

Name	$C_{[3.6\text{-}5.8\mu m]}$	σ_{c-}	σ_{c+}	$C_{[3.6\text{-}8.0\mu m]}$	σ_{c-}	σ_{c+}	$C_{[4.5\text{-}8.0\mu m]}$	σ_{c-}	σ_{c+}
COROT-2b				0.179	0.221	0.221	-0.179	0.217	0.217
GJ-436b	0.197	0.858	0.858	0.807	0.741	0.741	1.958	1.098	1.098
HAT-P-1b	1.010	0.198	0.198	1.205	0.212	0.212	0.642	0.254	0.254
HAT-P-7b	1.003	0.233	0.233	0.923	0.314	0.314	0.389	0.292	0.292
HD149026b	0.083	0.241	0.241	0.264	0.154	0.154	0.504	0.242	0.242
HD189733b	0.789	0.123	0.123	1.014	0.045	0.045	0.834	0.245	0.245
HD209458b	1.267	0.187	0.187	0.991	0.122	0.122	0.102	0.099	0.099
TrES-1				1.084	0.240	0.240	1.385	0.276	0.276
TrES-2	0.484	0.345	0.345	1.151	0.255	0.255	0.516	0.214	0.214
TrES-3	0.247	0.258	0.258	0.337	0.150	0.150	0.300	0.189	0.189
TrES-4	0.703	0.260	0.260	0.936	0.174	0.174	0.852	0.191	0.191
WASP-1b	0.958	0.275	0.275	1.531	0.183	0.183	0.886	0.151	0.151
WASP-2b	0.893	0.632	0.632	1.367	0.510	0.510	0.624	0.250	0.250
WASP-12b	0.554	0.097	0.097	0.580	0.162	0.162	0.547	0.142	0.142
WASP-18b	0.348	0.145	0.145	0.411	0.105	0.105	0.145	0.114	0.114
WASP-19b	0.200	0.101	0.095	0.250	0.197	0.194	0.089	0.200	0.200
XO-1b	1.201	0.156	0.156	0.993	0.174	0.174	0.623	0.170	0.170
XO-2b	0.768	0.327	0.327	0.565	0.460	0.460	0.386	0.457	0.457
XO-3b	0.316	0.399	0.399	0.450	0.264	0.264	0.062	0.265	0.265

TABLE 5
Parent Star Colors

Name	$C_{[3.6\text{-}4.5\mu m]}$	$C_{[4.5\text{-}5.8\mu m]}$	$C_{[5.8\text{-}8.0\mu m]}$	$C_{[3.6\text{-}5.8\mu m]}$	$C_{[3.6\text{-}8.0\mu m]}$	$C_{[4.5\text{-}8.0\mu m]}$
COROT-1	-0.00576	0.00439	0.02331	-0.00137	0.02194	0.0277
COROT-2	-0.01411	0.00704	0.03188	-0.00707	0.02481	0.03892
GJ-436	0.04245	0.0513	0.07545	0.09375	0.1692	0.12675
HAT-P-1	-0.00484	0.00412	0.02247	-0.00072	0.02175	0.02659
HAT-P-5	-0.00611	0.00444	0.02343	-0.00167	0.02176	0.02787
HAT-P-6	0.01319	-0.00251	0.00869	0.01068	0.01937	0.00618
HAT-P-7	0.00817	-0.00008	0.01254	0.0081	0.02064	0.01247
HAT-P-8	0.00372	0.00185	0.01589	0.00556	0.02146	0.01774
HD149026	0.00172	0.00237	0.01739	0.0041	0.02149	0.01976
HD189733	-0.0342	0.01288	0.04947	-0.02132	0.02815	0.06235
HD209458	0.00059	0.00267	0.01823	0.00326	0.0215	0.0209
Kepler-5	0.00662	0.00059	0.01371	0.00721	0.02092	0.01431
Kepler-6	-0.01677	0.00719	0.03413	-0.00957	0.02456	0.04132
Kepler-12	-0.03083	0.01029	0.04798	-0.02054	0.02744	0.05826
Kepler-17	-0.00488	0.00413	0.0225	-0.00075	0.02175	0.02663
TrES-1	-0.02683	0.01049	0.04322	-0.01634	0.02689	0.05372
TrES-2	-0.0095	0.00548	0.02676	-0.00402	0.02274	0.03224
TrES-3	-0.0109	0.00615	0.02872	-0.00476	0.02397	0.03487
TrES-4	-0.00005	0.00284	0.01872	0.00279	0.02151	0.02156
WASP-1	0.00033	0.00274	0.01843	0.00307	0.0215	0.02117
WASP-2	-0.02863	0.01098	0.04515	-0.01765	0.02749	0.05612
WASP-4	-0.02175	0.00824	0.03939	-0.0135	0.02589	0.04763
WASP-12	0.00521	0.0012	0.01477	0.00641	0.02118	0.01597
WASP-14	0.01122	-0.00151	0.01022	0.00971	0.01993	0.00871
WASP-18	0.00961	-0.0007	0.01146	0.00891	0.02037	0.01076
WASP-19	-0.02178	0.00825	0.03942	-0.01353	0.02589	0.04767
XO-1	-0.00992	0.00587	0.02775	-0.00404	0.02371	0.03362
XO-2	-0.02742	0.00949	0.045	-0.01794	0.02706	0.05448
XO-3	0.01024	-0.00101	0.01097	0.00922	0.0202	0.00996
XO-4	0.00953	-0.00066	0.01152	0.00887	0.02039	0.01086

TABLE 6
Brown Dwarf Spectral Types and Magnitudes

Name	Type	$M_{3.6\mu m}$	$\sigma_{3.6\mu m}$	$M_{4.5\mu m}$	$\sigma_{4.5\mu m}$	$M_{5.8\mu m}$	$\sigma_{5.8\mu m}$	$M_{8.0\mu m}$	$\sigma_{8.0\mu m}$	Ref. #
2MASS 0036+1821	L4	10.19	0.03	10.24	0.03	10.10	0.03	10.06	0.03	1, 2
2MASS 0050-3322	T7	14.82	0.03	13.57	0.03	13.32	0.03	13.00	0.04	3, 4
2MASS 0141+1804	L4.5	11.89	0.04	11.92	0.01	11.76	0.04	11.67	0.03	5, 2
2MASS 0243-2453	T6	13.90	0.03	12.95	0.04	12.71	0.05	12.27	0.05	3, 2
2MASS 0320-0446	L0.5	11.50	0.03	11.44	0.01	11.29	0.02	11.18	0.01	5, 2
2MASS 0348-6022	T7	14.04	0.03	12.51	0.03	12.89	0.03	12.28	0.04	3, 4
2MASS 0415-0935	T8	14.10	0.04	12.29	0.03	12.87	0.07	12.11	0.05	3, 2
2MASS 0451-3402	L0.5	11.66	0.04	11.66	0.03	11.52	0.02	11.30	0.04	6, 2
2MASS 0532+8246	L9.5	13.37	0.03	13.22	0.02	13.23	0.10	13.03	0.10	7, 2
2MASS 0559-1404	T4.5	12.67	0.03	11.93	0.03	11.73	0.03	11.42	0.03	3, 2
2MASS 0652+4710	L4.5	10.50	0.01	10.50	0.01	10.23	0.01	10.12	0.02	8, 2
2MASS 0717+5705	L6	11.95	0.01	11.96	0.01	11.76	0.01	11.68	0.01	5, 2
2MASS 0727+1710	T7	14.41	0.03	13.01	0.03	13.24	0.06	12.64	0.11	3, 2
2MASS 0746+2000AB	L1	9.86	0.03	9.90	0.05	9.72	0.03	9.57	0.03	1, 2
2MASS 0755+2212	T5	14.34	0.04	13.45	0.04	13.48	0.10	12.93	0.22	3, 2
2MASS 0825+2115	L6	11.70	0.03	11.59	0.03	11.16	0.03	10.93	0.03	1, 2
2MASS 0835-0819	L5	10.06	0.03	10.06	0.02	9.79	0.01	9.73	0.00	8, 2
2MASS 0908+5032	L9	11.67	0.03	11.66	0.03	11.39	0.03	11.13	0.04	9, 2
2MASS 0937+2931	T6	13.10	0.04	11.64	0.05	12.32	0.03	11.73	0.05	3, 2
2MASS 0939-2448AB	T8	13.76	0.04	11.66	0.04	12.95	0.04	11.89	0.04	3, 10
2MASS 1017+1308	L2	12.03	0.01	12.05	0.03	11.85	0.04	11.70	0.03	8, 2
2MASS 1047+2124	T6.5	14.39	0.06	12.95	0.05	13.52	0.07	12.91	0.10	3, 2
2MASS 1114-2618	T7.5	14.01	0.03	12.23	0.03	13.22	0.03	12.25	0.04	3, 4
2MASS 1155-3727	L2	10.74	0.02	10.75	0.02	10.58	0.01	10.42	0.02	11, 2
2MASS 1204+3212	L0	11.93	0.01	11.95	0.01	11.82	0.01	11.65	0.03	8, 2
2MASS 1209-1004AB	T3	13.94	0.03	13.45	0.03	13.34	0.11	13.11	0.10	3, 2
2MASS 1217-0311	T7.5	14.19	0.04	13.23	0.03	13.34	0.07	12.95	0.18	3, 2
2MASS 1225-2739AB	T6	13.84	0.03	12.75	0.03	12.84	0.10	12.24	0.03	3, 2
2MASS 1237+6526	T6.5	14.39	0.03	12.93	0.03	13.42	0.06	12.78	0.11	3, 2
2MASS 1300+1912	L1	10.96	0.02	11.00	0.03	10.86	0.01	10.73	0.03	12, 2
2MASS 1439+1929	L1	10.91	0.02	10.93	0.03	10.82	0.03	10.67	0.02	13, 2
2MASS 1506+1321	L3	10.86	0.02	10.85	0.06	10.69	0.02	10.58	0.01	12, 2
2MASS 1507-1627	L5.5	10.27	0.03	10.40	0.03	10.14	0.03	9.99	0.03	9, 2
2MASS 1515+4847	L6	11.31	0.02	11.33	0.02	11.07	0.02	10.83	0.02	5, 2
2MASS 1526+2043	L7	12.79	0.02	12.87	0.03	12.60	0.11	12.32	0.04	14, 2
2MASS 1534-2952AB	T5.5	13.63	0.05	12.71	0.03	12.73	0.05	12.36	0.08	3, 2
2MASS 1546-3325	T5.5	14.22	0.05	13.39	0.03	13.44	0.15	13.38	0.10	15, 2

TABLE 6 – *Continued*

Name	Type	$M_{3.6\mu m}$	$\sigma_{3.6\mu m}$	$M_{4.5\mu m}$	$\sigma_{4.5\mu m}$	$M_{5.8\mu m}$	$\sigma_{5.8\mu m}$	$M_{8.0\mu m}$	$\sigma_{8.0\mu m}$	Ref. #
2MASS 1553+1532AB	T7	14.42	0.03	13.08	0.03	13.30	0.10	12.65	0.10	3, 2
2MASS 1555-0956	L1	10.83	0.01	10.88	0.01	10.76	0.02	10.63	0.01	11, 2
2MASS 1632+1904	L7.5	12.70	0.03	12.65	0.03	12.24	0.05	12.00	0.05	1, 2
2MASS 1645-1319	L1.5	10.48	0.04	10.52	0.02	10.36	0.01	10.20	0.01	11, 2
2MASS 1721+3344	L3	11.58	0.02	11.62	0.02	11.49	0.04	11.40	0.02	8, 2
2MASS 1728+3948	L7	12.72	0.02	12.66	0.01	12.29	0.04	12.13	0.03	14, 2
2MASS 1835+3259	M8.5	8.55	0.02	8.55	0.01	8.39	0.01	8.29	0.01	16, 2
2MASS 2104-1037	L3	11.55	0.03	11.62	0.01	11.44	0.03	11.29	0.04	8, 2
2MASS 2224-0158	L3.5	11.05	0.03	11.14	0.03	10.85	0.03	10.81	0.03	9, 2
2MASS 2244+2043	L7.5	12.35	0.03	12.11	0.03	11.59	0.03	11.36	0.03	9, 17
2MASS 2254+3123	T4	13.93	0.03	13.28	0.03	13.03	0.10	12.78	0.10	3, 2
2MASS 2339+1352	T5	14.82	0.05	13.95	0.05	13.98	0.04	13.80	0.20	3, 2
2MASS 2356-1553	T5.5	14.69	0.04	13.69	0.03	13.57	0.08	13.21	0.17	3, 2
BRI0021-0214	M9.5	9.94	0.03	9.91	0.03	9.72	0.03	9.55	0.03	1, 2
DEN0021-4244	M9.5	11.62	0.01	11.59	0.01	11.43	0.04	11.30	0.04	6, 2
DEN0255-4700	L9	10.29	0.02	10.20	0.02	9.89	0.01	9.61	0.01	3, 2
DEN1058-1548	L3	11.76	0.03	11.77	0.03	11.60	0.03	11.50	0.03	1, 2
DEN1539-0520	L4	11.65	0.02	11.75	0.04	11.61	0.05	11.60	0.05	18, 2
ε Ind BC	T3.5	9.97	0.01	9.44	0.02	9.39	0.03	8.98	0.04	15, 2
GJ-1001A	M3.5	7.45	0.03	7.40	0.03	7.37	0.01	7.36	0.01	19, 2
GJ-1001BC	L5	10.36	0.01	10.47	0.01	10.14	0.03	10.13	0.02	20, 2
GJ-1002	M5.5	7.07	0.01	7.01	0.01	6.97	0.02	6.95	0.01	21, 2
GJ-1093	M5	7.86	0.03	7.84	0.02	7.76	0.01	7.74	0.01	21, 2
GJ-1111	M6.5	6.84	0.02	6.84	0.04	6.76	0.05	6.74	0.01	22, 2
GJ-1156	M5	7.24	0.03	7.16	0.02	7.10	0.01	7.08	0.01	21, 2
GJ-337CD	L8	12.50	0.02	12.33	0.02	11.96	0.08	11.95	0.05	23, 2
GJ-412B	M5.5	7.38	0.01	7.29	0.05	7.23	0.02	7.18	0.00	21, 2
GJ-570D	T7.5	13.80	0.04	12.12	0.02	12.77	0.11	11.97	0.07	15, 2
GJ-644C	M7	8.37	0.02	8.38	0.01	8.28	0.02	8.24	0.02	22, 2
GJ-752B	M8	8.29	0.02	8.30	0.03	8.15	0.01	8.14	0.00	22, 2
GL 570D	T7.5	13.80	0.05	12.12	0.03	12.77	0.11	11.97	0.07	3, 2
HD 3651B	T7.5	15.38	0.04	13.62	0.02	14.04	0.12	13.45	0.14	24, 24
HN PegB	T2.5	13.72	0.04	13.39	0.02	13.08	0.10	12.58	0.11	24, 24
Kelu-1AB	L3	10.92	0.06	10.90	0.05	10.73	0.03	10.61	0.03	1, 2
LHS 102A	M3.5	7.45	0.03	7.40	0.03	7.37	0.03	7.36	0.03	25, 2
LHS 102BC	L4.5	10.36	0.03	10.47	0.03	10.14	0.03	10.13	0.03	9, 2
LHS 132	M8	9.64	0.02	9.62	0.02	9.52	0.02	9.48	0.01	26, 2

TABLE 6 – *Continued*

Name	Type	$M_{3.6\mu m}$	$\sigma_{3.6\mu m}$	$M_{4.5\mu m}$	$\sigma_{4.5\mu m}$	$M_{5.8\mu m}$	$\sigma_{5.8\mu m}$	$M_{8.0\mu m}$	$\sigma_{8.0\mu m}$	Ref. #
LHS 2021	M8	10.32	0.02	10.35	0.01	10.24	0.01	10.20	0.01	27, 2
LHS 2065	M9	9.41	0.03	9.39	0.03	9.22	0.03	9.13	0.03	1, 2
LHS 288	M5.5	7.31	0.03	7.25	0.04	7.27	0.01	7.20	0.01	28, 2
LHS 292	M6.5	7.51	0.03	7.51	0.03	7.46	0.03	7.42	0.03	1, 2
LHS 2924	M9	10.16	0.03	10.16	0.03	9.97	0.03	9.81	0.03	29, 2
LHS 3003	M7	8.47	0.03	8.49	0.03	8.39	0.03	8.36	0.03	1, 2
LP944-020	M9	8.87	0.03	8.79	0.01	8.59	0.01	8.42	0.01	30, 2
SDSS 0000+2554	T4.5	13.72	0.03	13.07	0.03	12.56	0.09	12.50	0.03	3, 17
SDSS 0151+1244	T1	14.06	0.03	13.91	0.03	13.62	0.11	13.34	0.18	1, 2
SDSS 0207+0000	T4.5	15.59	0.06	14.98	0.05	14.67	0.20	14.17	0.19	3, 2
SDSS 0423-0414AB	T0	11.73	0.03	11.58	0.03	11.30	0.03	11.01	0.03	3, 2
SDSS 0539-0059	L5	11.49	0.03	11.60	0.03	11.35	0.04	11.20	0.05	1, 2
SDSS 0758+3247	T2	12.41	0.03	12.13	0.03	11.71	0.03	11.33	0.04	3, 17
SDSS 0805+4812	L9.5	12.44	0.03	12.43	0.03	12.32	0.03	12.10	0.03	9, 17
SDSS 0837-0000	T1	14.76	0.03	14.60	0.03	14.41	0.13	14.22	0.14	3, 2
SDSS 0857+5708	L8	11.62	0.03	11.44	0.03	11.02	0.03	10.74	0.03	1, 2
SDSS 0926+5847AB	T4.5	14.48	0.03	13.71	0.03	13.55	0.11	13.32	0.06	3, 2
SDSS 1021-0304AB	T3	14.16	0.03	13.80	0.03	13.58	0.12	13.16	0.11	3, 2
SDSS 1052+4422AB	T0.5	13.23	0.03	13.10	0.03	12.67	0.03	12.36	0.03	31, 17
SDSS 1110+0116	T5.5	14.71	0.04	13.88	0.03	13.43	0.07	13.21	0.16	3, 2
SDSS 1155+0559	L7.5	12.83	0.03	12.83	0.03	12.50	0.03	12.26	0.03	9, 17
SDSS 1207+0244	T0	12.86	0.03	12.73	0.03	12.42	0.03	12.23	0.06	3, 17
SDSS 1254-0122	T2	12.63	0.03	12.39	0.03	11.99	0.05	11.75	0.05	3, 2
SDSS 1331-0116	L8	12.96	0.03	13.13	0.03	12.95	0.08	12.62	0.06	9, 2
SDSS 1346-0031	T6.5	14.53	0.05	13.60	0.03	13.40	0.11	13.13	0.17	3, 2
SDSS 1504+1027	T7	15.44	0.03	14.01	0.03	14.37	0.04	13.76	0.07	31, 4
SDSS 1516+3053	T0.5	13.61	0.03	13.39	0.03	12.89	0.03	12.47	0.03	31, 17
SDSS 1520+3546	T0	12.94	0.03	12.89	0.03	12.49	0.03	12.26	0.03	31, 17
SDSS 1624+0029	T6	14.30	0.04	13.08	0.03	13.25	0.08	12.84	0.09	3, 2
SDSS 1628+2308	T7	15.25	0.03	13.86	0.03	14.14	0.05	13.55	0.07	31, 4
SDSS 1750+1759	T3.5	14.95	0.03	14.46	0.03	14.15	0.23	13.93	0.23	3, 2
SDSS 2028+0052	L3	11.97	0.02	12.03	0.02	11.83	0.03	11.71	0.03	32, 2
SO 0253+1652	M7	7.12	0.01	7.10	0.02	7.05	0.01	7.02	0.01	27, 2
ULAS 0034-0052	T9	16.28	0.03	14.49	0.03	14.82	0.05	13.91	0.06	33, 34
ULAS 0139+0048	T7.5	17.59	0.04	16.33	0.03					35, 4
ULAS 0150+1359	T7.5	16.42	0.03	15.12	0.03					36, 4
ULAS 0857+0913	T6	17.65	0.03	16.73	0.03	16.50	0.10	16.36	0.31	36, 4

TABLE 6 – *Continued*

Name	Type	$M_{3.6\mu m}$	$\sigma_{3.6\mu m}$	$M_{4.5\mu m}$	$\sigma_{4.5\mu m}$	$M_{5.8\mu m}$	$\sigma_{5.8\mu m}$	$M_{8.0\mu m}$	$\sigma_{8.0\mu m}$	Ref. #
ULAS 1017+0118	T8	17.29	0.03	16.02	0.03	15.90	0.04	15.70	0.15	33, 4
ULAS 1238+0953	T8.5	17.09	0.03	15.34	0.03	15.32	0.06	14.58	0.10	33, 4
ULAS 1335+1130	T9	15.95	0.03	13.91	0.03	14.34	0.05	13.37	0.06	33
ULAS 2146-0010	T8.5	16.44	0.03	14.43	0.03	15.38	0.15	14.36	0.08	37, 4
ULAS 2321+1354	T7.5	15.80	0.03	14.16	0.03					36, 4
WD 0806-661B	Y0[a]	19.70	0.15	16.85	0.05					38
WISE 0008-1739	T6	16.04	0.03	14.87	0.02					39
WISE 0049+0441	L9	12.98	0.02	12.95	0.02					39
WISE 0106+1518	M8	12.86	0.02	12.72	0.02					39
WISE 0123+4142	T7	16.13	0.03	14.85	0.02					39
WISE 0138-0322	T3	13.89	0.02	13.43	0.02					39
WISE 0148-7202	T9.5	16.84	0.05	14.65	0.02					39
WISE 0150+3827	T0	13.24	0.02	13.12	0.02					39
WISE 0206+2640	L9	13.08	0.02	12.87	0.02					39
WISE 0221+3842	T26.5	15.93	0.03	14.86	0.02					39
WISE 0223-2932	T7.25	15.81	0.03	14.02	0.02					39
WISE 0226-0211	T7	16.60	0.04	14.68	0.02					39
WISE 0254+0223	T8	14.69	0.02	12.71	0.02					39
WISE 0305+3954	T6	15.98	0.03	14.54	0.02					39
WISE 0307+2904	T6.5	16.39	0.04	14.97	0.02					39
WISE 0313+7807	T8.5	15.31	0.02	13.27	0.02					39
WISE 0323-6025	T8.5	16.57	0.04	14.51	0.02					39
WISE 0333-5856	T3	13.59	0.02	13.30	0.02					39
WISE 0410+1502	Y0	16.64	0.04	14.18	0.02					39
WISE 0410+1411	T6	16.10	0.03	15.00	0.02					39
WISE 0458+6434	T8.5	15.08	0.02	12.99	0.02					39
WISE 0500-1223	T8	15.95	0.03	14.00	0.02					39
WISE 0513+0608	T6.5	15.11	0.02	13.95	0.02					39
WISE 0525+6739	T6	16.40	0.04	14.88	0.02					39
WISE 0528-3308	T7	16.31	0.03	14.59	0.02					39
WISE 0539-1034	T5.5	16.15	0.03	15.01	0.02					39
WISE 0542-1628	T6.5	15.27	0.02	13.97	0.02					39
WISE 0611-0410	T0	13.07	0.02	12.92	0.02					39
WISE 0612-3036	T6	15.59	0.03	14.03	0.02					39
WISE 0612-4920	T3.5	14.73	0.02	14.13	0.02					39
WISE 0614+3912	T6	15.19	0.02	13.60	0.02					39
WISE 0623-0456	T8	15.49	0.03	13.74	0.02					39
WISE 0625+5646	T6	15.47	0.03	14.41	0.02					39

TABLE 6 – *Continued*

Name	Type	$M_{3.6\mu m}$	$\sigma_{3.6\mu m}$	$M_{4.5\mu m}$	$\sigma_{4.5\mu m}$	Ref. #
WISE 0627-1114	T6	14.27	0.02	13.33	0.02	39
WISE 0750+2725	T8.5	16.68	0.04	14.49	0.02	39
WISE 0751-7634	T9	16.43	0.04	14.62	0.02	39
WISE 0759-4904	T8	15.62	0.03	13.76	0.02	39
WISE 0819-0335	T4	13.61	0.02	13.07	0.02	39
WISE 0836-1859	T8	16.88	0.05	15.09	0.02	39
WISE 0857+5604	T8	16.03	0.03	14.14	0.02	39
WISE 0906+4735	T8	16.47	0.04	14.55	0.02	39
WISE 0929+0409	T6.5	15.72	0.03	14.24	0.02	39
WISE 0952+1955	T6	15.82	0.03	14.50	0.02	39
WISE 1018-2445	T8	16.13	0.03	14.14	0.02	39
WISE 1019+6529	T6	15.31	0.02	14.00	0.02	39
WISE 1042-3842	T8.5	16.77	0.04	14.57	0.02	39
WISE 1122+2550	T6	15.37	0.02	14.06	0.02	39
WISE 1150+6302	T8	15.61	0.03	13.43	0.02	39
WISE 1217+1626	T9	15.44	0.02	13.11	0.02	39
WISE 1311+0122	T9	16.82	0.05	14.68	0.02	39
WISE 1311+3629	L5	13.16	0.02	13.19	0.02	39
WISE 1320+6034	T6.5	15.83	0.03	14.50	0.02	39
WISE 1322-2340	T8	15.67	0.03	13.89	0.02	39
WISE 1348+6603	L9	13.95	0.02	13.82	0.02	39
WISE 1405+5534	Y0	16.88	0.05	14.06	0.02	39
WISE 1436-1814	T8	15.99	0.03	14.72	0.02	39
WISE 1457+5815	T7	15.85	0.03	14.44	0.02	39
WISE 1506+7027	T6	12.63	0.02	11.32	0.02	39
WISE 1519+7009	T8	16.19	0.03	14.09	0.02	39
WISE 1541-2250	Y0	16.73	0.04	14.23	0.02	39
WISE 1612-3420	T6.5	15.45	0.03	13.86	0.02	39
WISE 1614+1739	T9	16.43	0.04	14.22	0.02	39
WISE 1617+1807	T8	15.96	0.03	14.10	0.02	39
WISE 1622-0959	T6	15.36	0.02	14.15	0.02	39
WISE 1627+3255	T6	15.22	0.02	13.62	0.02	39
WISE 1647+5632	L0	13.25	0.02	13.13	0.02	39
WISE 1653+4444	T8	15.67	0.03	13.87	0.02	39
WISE 1711+3500	T8	16.46	0.04	14.62	0.02	39
WISE 1717+6129	T8	17.06	0.05	15.13	0.02	39
WISE 1728+5716	T6	16.47	0.04	14.99	0.02	39

TABLE 6 – *Continued*

Name	Type	$M_{3.6\mu m}$	$\sigma_{3.6\mu m}$	$M_{4.5\mu m}$	$\sigma_{4.5\mu m}$	Ref. #
WISE 1738+2732	Y0	17.10	0.05	14.48	0.02	39
WISE 1741+2553	T9	14.43	0.02	12.39	0.02	39
WISE 1804+3117	T9.5	16.62	0.04	14.60	0.02	39
WISE 1828+2650	Y0	16.92	0.02	14.32	0.02	39
WISE 1841+7000	T5	15.63	0.03	14.33	0.02	39
WISE 1852+3537	T7	15.59	0.03	14.19	0.02	39
WISE 1952+7240	T4	14.05	0.02	13.20	0.02	39
WISE 2056+1459	Y0	16.04	0.03	13.92	0.02	39
WISE 2134-7131	T9	16.18	0.03	13.96	0.02	39
WISE 2157+2659	T7	16.01	0.03	14.44	0.02	39
WISE 2209-2734	T7	15.48	0.03	13.90	0.02	39
WISE 2213+0911	T7	15.80	0.03	14.57	0.02	39
WISE 2226+0440	T8.5	16.12	0.03	14.55	0.02	39
WISE 2237-0614	T5	16.16	0.03	14.93	0.02	39
WISE 2239+1617	T3	14.15	0.02	13.55	0.02	39
WISE 2255-3118	T8	15.92	0.03	14.21	0.02	39
WISE 2319-1844	T7.5	15.92	0.03	13.95	0.02	39
WISE 2325-4105	T9	16.27	0.03	14.09	0.02	39
WISE 2327-2730	L9	13.58	0.02	13.34	0.02	39
WISE 2340-0745	T7	15.20	0.02	13.63	0.02	39
WISE 2344+1034	T9	16.73	0.04	14.91	0.02	39
WISE 2348-1028	T7	15.87	0.03	14.36	0.02	39
WISE 2359-7335	T5.5	14.48	0.02	13.38	0.02	39

REFERENCES. — (1) Geballe et al. (2002); (2) Patten et al. (2006); (3) Burgasser et al. (2006); (4) Leggett et al. (2010); (5) Wilson et al. (2003); (6) Basri et al. (2000); (7) Burgasser et al. (2003); (8) Cruz et al. (2003); (9) Knapp et al. (2004); (10) Burgasser et al. (2008); (11) Gizis (2002); (12) Gizis et al. (2000); (13) Kirkpatrick et al. (1999); (14) Kirkpatrick et al. (2000); (15) Burgasser et al. (2005); (16) Reid et al. (2003); (17) Leggett et al. (2007); (18) Kirkpatrick et al. (2006); (19) Golimowski et al. (2004); (20) Kirkpatrick et al. (2001); (21) Henry et al. (1999); (22) Kirkpatrick et al. (1991); (23) Wilson et al. (2001); (24) Luhman et al. (2007); (25) Bidelman (1985); (26) Scholz et al. (2000); (27) Henry et al. (2004); (28) Bessell (1991); (29) Leggett (1992); (30) Kirkpatrick et al. (1997); (31) Chiu et al. (2006); (32) Hawley et al. (2002); (33) Burningham et al. (2008); (34) Warren et al. (2007); (35) Chiu et al. (2008); (36) Burningham et al. (2010); (37) Burningham et al. (2009); (38) Luhman et al. (2012); (39) Kirkpatrick et al. (2011).

[a]Estimated from T_{err} described in Luhman et al. (2012), using the relationship described in Stephens et al. (2009) and in Section III of this work.

TABLE 7A
Brown Dwarf Effective Temperatures and Colors

Name	T_{eff} (K)	$C_{[3.6-4.5\mu m]}$	σ_c	$C_{[4.5-5.8\mu m]}$	σ_c	$C_{[5.8-8.0\mu m]}$	σ_c
2MASS 0036+1821	1715	-0.05	0.04	0.14	0.04	0.04	0.04
2MASS 0050-3322	884	1.25	0.04	0.25	0.04	0.32	0.05
2MASS 0141+1804	1660	-0.03	0.04	0.16	0.04	0.09	0.05
2MASS 0243-2453	1007	0.95	0.05	0.24	0.06	0.44	0.07
2MASS 0320-0446	2182	0.06	0.03	0.15	0.02	0.11	0.02
2MASS 0348-6022	884	1.53	0.04	-0.38	0.04	0.61	0.05
2MASS 0415-0935	717	1.81	0.05	-0.58	0.08	0.76	0.09
2MASS 0451-3402	2182	0.00	0.05	0.14	0.04	0.22	0.04
2MASS 0532+8246	1320	0.15	0.04	-0.01	0.10	0.20	0.14
2MASS 0559-1404	1130	0.74	0.04	0.20	0.04	0.31	0.04
2MASS 0652+4710	1660	0.00	0.01	0.27	0.01	0.11	0.02
2MASS 0717+5705	1520	-0.01	0.01	0.20	0.01	0.08	0.01
2MASS 0727+1710	884	1.40	0.04	-0.23	0.07	0.60	0.13
2MASS 0746+2000AB	2109	-0.04	0.06	0.18	0.06	0.15	0.04
2MASS 0755+2212	1096	0.89	0.06	-0.03	0.11	0.55	0.24
2MASS 0825+2115	1520	0.11	0.04	0.43	0.04	0.23	0.04
2MASS 0835-0819	1610	0.00	0.04	0.27	0.02	0.06	0.01
2MASS 0908+5032	1340	0.01	0.04	0.27	0.04	0.26	0.05
2MASS 0937+2931	1007	1.46	0.06	-0.68	0.06	0.59	0.06
2MASS 0939-2448AB	717	2.10	0.06	-1.29	0.06	1.06	0.06
2MASS 1017+1308	1967	-0.02	0.03	0.20	0.05	0.15	0.05
2MASS 1047+2124	950	1.44	0.08	-0.57	0.09	0.61	0.12
2MASS 1114-2618	807	1.78	0.04	-0.99	0.04	0.97	0.05
2MASS 1155-3727	1967	-0.01	0.03	0.17	0.02	0.16	0.02
2MASS 1204+3212	2256	-0.02	0.01	0.13	0.01	0.17	0.03
2MASS 1209-1004AB	1205	0.49	0.04	0.11	0.11	0.23	0.15
2MASS 1217-0311	807	0.96	0.05	-0.11	0.08	0.39	0.19
2MASS 1225-2739AB	1007	1.09	0.04	-0.09	0.10	0.60	0.10
2MASS 1237+6526	950	1.46	0.04	-0.49	0.07	0.64	0.13
2MASS 1300+1912	2109	-0.04	0.04	0.14	0.03	0.13	0.03
2MASS 1439+1929	2109	-0.02	0.04	0.11	0.04	0.15	0.04
2MASS 1506+1321	1835	0.01	0.06	0.16	0.06	0.11	0.02
2MASS 1507-1627	1563	-0.13	0.04	0.26	0.04	0.15	0.04
2MASS 1515+4847	1520	-0.02	0.03	0.26	0.03	0.24	0.03
2MASS 1526+2043	1446	-0.08	0.04	0.27	0.11	0.28	0.12
2MASS 1534-2952AB	1055	0.92	0.06	-0.02	0.06	0.37	0.09
2MASS 1546-3325	1055	0.83	0.06	-0.05	0.15	0.06	0.18

TABLE 7A – *Continued*

Name	T_{eff} (K)	$C_{[3.6-4.5\mu m]}$	σ_c	$C_{[4.5-5.8\mu m]}$	σ_c	$C_{[5.8-8.0\mu m]}$	σ_c
2MASS 1553+1532AB	884	1.34	0.04	-0.22	0.10	0.65	0.14
2MASS 1555-0956	2109	-0.05	0.01	0.12	0.02	0.13	0.02
2MASS 1632+1904	1415	0.05	0.04	0.41	0.06	0.24	0.07
2MASS 1645-1319	2037	-0.04	0.04	0.16	0.02	0.16	0.01
2MASS 1721+3344	1835	-0.04	0.03	0.13	0.04	0.09	0.04
2MASS 1728+3948AB	1446	0.06	0.02	0.37	0.04	0.16	0.05
2MASS 1835+3259	2475	0.00	0.02	0.16	0.01	0.10	0.01
2MASS 2104-1037	1835	-0.07	0.03	0.18	0.03	0.15	0.05
2MASS 2224-0158	1773	-0.09	0.04	0.29	0.04	0.04	0.04
2MASS 2244+2043	1415	0.24	0.04	0.52	0.04	0.23	0.04
2MASS 2254+3123	1159	0.65	0.04	0.25	0.10	0.25	0.14
2MASS 2339+1352	1096	0.87	0.07	-0.03	0.06	0.18	0.20
2MASS 2356-1553	1055	1.00	0.05	0.12	0.09	0.36	0.19
BRI0021-0214	2330	0.03	0.04	0.19	0.04	0.17	0.04
DEN0021-4244	2330	0.03	0.01	0.16	0.04	0.13	0.06
DEN0255-4700	1340	0.09	0.03	0.31	0.02	0.28	0.01
DEN1058-1548	1835	-0.01	0.04	0.17	0.04	0.10	0.04
DEN1539-0520	1715	-0.10	0.04	0.14	0.06	0.01	0.07
eps Ind BC	1184	0.53	0.02	0.05	0.04	0.41	0.05
GJ-1001A	2867	0.05	0.04	0.03	0.03	0.01	0.01
GJ-1001BC	1610	-0.11	0.01	0.33	0.03	0.01	0.04
GJ-1002	2816	0.06	0.01	0.04	0.02	0.02	0.02
GJ-1093	2847	0.02	0.04	0.08	0.02	0.02	0.01
GJ-1111	2727	0.00	0.04	0.08	0.06	0.02	0.05
GJ-1156	2847	0.08	0.04	0.06	0.02	0.02	0.01
GJ-337CD	1387	0.17	0.03	0.37	0.08	0.01	0.09
GJ-412B	2816	0.09	0.05	0.06	0.05	0.05	0.02
GJ-570D	807	1.68	0.04	-0.65	0.11	0.80	0.13
GJ-644C	2672	-0.01	0.02	0.10	0.02	0.04	0.03
GJ-752B	2544	-0.01	0.04	0.15	0.03	0.01	0.01
GL 570D	807	1.68	0.06	-0.65	0.11	0.80	0.13
HD 3651B	807	1.76	0.04	-0.42	0.12	0.59	0.18
HN PegB	1224	0.33	0.04	0.31	0.10	0.50	0.15
Kelu-1AB	1835	0.02	0.08	0.17	0.06	0.12	0.04
LHS 102A	2867	0.05	0.04	0.03	0.04	0.01	0.04
LHS 102BC	1660	-0.11	0.04	0.33	0.04	0.01	0.04
LHS 132	2544	0.02	0.03	0.10	0.03	0.04	0.02

TABLE 7A – *Continued*

Name	T_{eff} (K)	$C_{[3.6-4.5\mu m]}$	σ_c	$C_{[4.5-5.8\mu m]}$	σ_c	$C_{[5.8-8.0\mu m]}$	σ_c
LHS 2021	2544	-0.03	0.02	0.11	0.01	0.04	0.01
LHS 2065	2403	0.02	0.04	0.17	0.04	0.09	0.04
LHS 288	2816	0.06	0.05	-0.02	0.04	0.07	0.01
LHS 292	2727	0.00	0.04	0.05	0.04	0.04	0.04
LHS 2924	2403	0.00	0.04	0.19	0.04	0.16	0.04
LHS 3003	2672	-0.02	0.04	0.10	0.04	0.03	0.04
LP944-020	2403	0.08	0.03	0.20	0.01	0.17	0.01
SDSS 0000+2554	1130	0.65	0.04	0.51	0.09	0.06	0.09
SDSS 0151+1244	1271	0.15	0.04	0.29	0.11	0.28	0.21
SDSS 0207+0000	1130	0.61	0.08	0.31	0.21	0.50	0.28
SDSS 0423-0414AB	1302	0.15	0.04	0.28	0.04	0.29	0.04
SDSS 0539-0059	1610	-0.11	0.04	0.25	0.05	0.15	0.06
SDSS 0758+3247	1240	0.28	0.04	0.42	0.04	0.38	0.05
SDSS 0805+4812	1320	0.01	0.04	0.11	0.04	0.22	0.04
SDSS 0837-0000	1271	0.16	0.04	0.19	0.13	0.19	0.19
SDSS 0857+5708	1387	0.18	0.04	0.42	0.04	0.28	0.04
SDSS 0926+5847AB	1130	0.77	0.04	0.16	0.11	0.23	0.13
SDSS 1021-0304AB	1205	0.36	0.04	0.22	0.12	0.42	0.16
SDSS 1052+4422AB	1286	0.13	0.04	0.43	0.04	0.31	0.04
SDSS 1110+0116	1055	0.83	0.05	0.45	0.08	0.22	0.17
SDSS 1155+0559	1415	0.00	0.04	0.33	0.04	0.24	0.04
SDSS 1207+0244	1302	0.13	0.04	0.31	0.04	0.19	0.07
SDSS 1254-0122	1240	0.24	0.04	0.40	0.06	0.24	0.07
SDSS 1331-0116	1387	-0.17	0.04	0.18	0.09	0.33	0.10
SDSS 1346-0031	950	0.93	0.06	0.20	0.11	0.27	0.20
SDSS 1504+1027	884	1.43	0.04	-0.36	0.05	0.61	0.08
SDSS 1516+3053	1286	0.22	0.04	0.50	0.04	0.42	0.04
SDSS 1520+3546	1302	0.05	0.04	0.40	0.04	0.23	0.04
SDSS 1624+0029	1007	1.22	0.05	-0.17	0.09	0.41	0.12
SDSS 1628+2308	884	1.39	0.04	-0.28	0.06	0.59	0.09
SDSS 1750+1759	1184	0.49	0.04	0.31	0.23	0.22	0.33
SDSS 2028+0052	1835	-0.06	0.03	0.20	0.04	0.12	0.04
SO 0253+1652	2672	0.02	0.02	0.05	0.02	0.03	0.01
ULAS 0034-0052	497	1.79	0.04	-0.33	0.06	0.91	0.08
ULAS 0139+0048	807	1.26	0.05				
ULAS 0150+1359	807	1.30	0.04				
ULAS 0857+0913	1007	0.92	0.04	0.23	0.10	0.14	0.33

TABLE 7A – *Continued*

Name	T_{eff} (K)	$C_{[3.6\text{-}4.5\mu m]}$	σ_c	$C_{[4.5\text{-}5.8\mu m]}$	σ_c	$C_{[5.8\text{-}8.0\mu m]}$	σ_c
ULAS 1017+0118	717	1.27	0.04	0.12	0.05	0.20	0.16
ULAS 1238+0953	615	1.75	0.04	0.02	0.07	0.74	0.12
ULAS 1335+1130	497	2.04	0.04	-0.43	0.06	0.97	0.08
ULAS 2146-0010	615	2.01	0.04	-0.95	0.15	1.02	0.17
ULAS 2321+1354	807	1.64	0.04				
WD 0806+661B	315[a]	2.85	0.16				
WISE 0008-1739	1007	1.18	0.04				
WISE 0049+0441	1340	0.03	0.02				
WISE 0106+1518	2544	0.15	0.02				
WISE 0123+4142	884	1.28	0.04				
WISE 0138-0322	1205	0.46	0.03				
WISE 0148-7202	364	2.19	0.05				
WISE 0150+3827	1302	0.12	0.02				
WISE 0206+2640	1340	0.21	0.02				
WISE 0221+3842	950	1.07	0.04				
WISE 0223-2932	847	1.80	0.03				
WISE 0226-0211	884	1.92	0.05				
WISE 0254+0223	717	1.98	0.03				
WISE 0305+3954	1007	1.44	0.04				
WISE 0307+2904	950	1.42	0.04				
WISE 0313+7807	615	2.04	0.03				
WISE 0323-6025	615	2.07	0.04				
WISE 0333-5856	1205	0.29	0.02				
WISE 0410+1502	214	2.46	0.05				
WISE 0410+1411	1007	1.10	0.04				
WISE 0458+6434	615	2.10	0.03				
WISE 0500-1223	717	1.95	0.03				
WISE 0513+0608	950	1.16	0.03				
WISE 0525+6739	1007	1.52	0.04				
WISE 0528-3308	884	1.72	0.04				
WISE 0539-1034	1055	1.14	0.04				
WISE 0542-1628	950	1.30	0.03				
WISE 0611-0410	1302	0.15	0.02				
WISE 0612-3036	1007	1.56	0.03				
WISE 0612-4920	1184	0.60	0.03				
WISE 0614+3912	1007	1.59	0.03				
WISE 0623-0456	717	1.76	0.03				

TABLE 7A – *Continued*

Name	T_{eff} (K)	$C_{[3.6-4.5\mu m]}$	σ_c	Name	Teff (K)	$C_{[3.6-4.5\mu m]}$	σ_c
WISE 0625+5646	1007	1.06	0.03	WISE 1728+5716	1007	1.48	0.04
WISE 0627-1114	1007	0.95	0.03	WISE 1738+2732	214	2.62	0.06
WISE 0750+2725	615	2.19	0.05	WISE 1741+2553	497	2.04	0.03
WISE 0751-7634	497	1.81	0.04	WISE 1804+3117	364	2.01	0.04
WISE 0759-4904	717	1.86	0.03	WISE 1828+2650	214	2.6	0.03
WISE 0819-0335	1159	0.54	0.02	WISE 1841+7000	1096	1.30	0.03
WISE 0836-1859	717	1.79	0.05	WISE 1852+3537	884	1.40	0.03
WISE 0857+5604	717	1.89	0.04	WISE 1952+7240	1159	0.85	0.03
WISE 0906+4735	717	1.92	0.04	WISE 2056+1459	214	2.11	0.03
WISE 0929+0409	950	1.48	0.03	WISE 2134-7131	497	2.22	0.04
WISE 0952+1955	1007	1.32	0.03	WISE 2157+2659	884	1.57	0.04
WISE 1018-2445	717	2.00	0.04	WISE 2209-2734	884	1.58	0.03
WISE 1019+6529	1007	1.31	0.03	WISE 2213+0911	884	1.23	0.03
WISE 1042-3842	615	2.20	0.05	WISE 2226+0440	615	1.58	0.04
WISE 1122+2550	1007	1.31	0.03	WISE 2237-0614	1096	1.24	0.04
WISE 1150+6302	717	2.19	0.03	WISE 2239+1617	1205	0.59	0.03
WISE 1217+1626	497	2.33	0.03	WISE 2255-3118	717	1.71	0.03
WISE 1311+0122	497	2.14	0.05	WISE 2319-1844	807	1.98	0.03
WISE 1311+3629	1610	-0.03	0.02	WISE 2325-4105	497	2.18	0.04
WISE 1320+6034	950	1.34	0.03	WISE 2327-2730	1340	0.25	0.03
WISE 1322-2340	717	1.77	0.03	WISE 2340-0745	884	1.57	0.03
WISE 1348+6603	1340	0.13	0.03	WISE 2344+1034	497	1.83	0.05
WISE 1405+5534	214	2.82	0.05	WISE 2348-1028	884	1.51	0.03
WISE 1436-1814	717	1.27	0.04	WISE 2359-7335	1055	1.10	0.03
WISE 1457+5815	884	1.41	0.03				
WISE 1506+7027	1007	1.31	0.02				
WISE 1519+7009	717	2.11	0.04				
WISE 1541-2250	214	2.50	0.05				
WISE 1612-3420	950	1.59	0.03				
WISE 1614+1739	497	2.21	0.04				
WISE 1617+1807	717	1.87	0.03				
WISE 1622-0959	1007	1.22	0.03				
WISE 1627+3255	1007	1.60	0.03				
WISE 1647+5632	1340	0.13	0.02				
WISE 1653+4444	717	1.80	0.03				
WISE 1711+3500	717	1.84	0.04				
WISE 1717+6129	717	1.93	0.06				

[a] T_{eff} for WD0806+661B from Luhman et al. (2012)

TABLE 7B
Other Brown Dwarf Colors

Name	$C_{[3.6\text{-}5.8\mu m]}$	σ_c	$C_{[3.6\text{-}8.0\mu m]}$	σ_c	$C_{[4.5\text{-}8.0\mu m]}$	σ_c
2MASS 0036+1821	0.09	0.04	0.13	0.04	0.18	0.04
2MASS 0050-3322	1.50	0.04	1.82	0.05	0.57	0.05
2MASS 0141+1804	0.13	0.06	0.22	0.05	0.25	0.03
2MASS 0243-2453	1.19	0.06	1.63	0.06	0.68	0.06
2MASS 0320-0446	0.21	0.04	0.32	0.03	0.26	0.01
2MASS 0348-6022	1.15	0.04	1.76	0.05	0.23	0.05
2MASS 0415-0935	1.23	0.08	1.99	0.06	0.18	0.06
2MASS 0451-3402	0.14	0.04	0.36	0.06	0.36	0.05
2MASS 0532+8246	0.14	0.10	0.34	0.10	0.19	0.10
2MASS 0559-1404	0.94	0.04	1.25	0.04	0.51	0.04
2MASS 0652+4710	0.27	0.01	0.38	0.02	0.38	0.02
2MASS 0717+5705	0.19	0.01	0.27	0.01	0.28	0.01
2MASS 0727+1710	1.17	0.07	1.77	0.11	0.37	0.11
2MASS 0746+2000AB	0.14	0.04	0.29	0.04	0.33	0.06
2MASS 0755+2212	0.86	0.11	1.41	0.22	0.52	0.22
2MASS 0825+2115	0.54	0.04	0.77	0.04	0.66	0.04
2MASS 0835-0819	0.27	0.03	0.33	0.03	0.33	0.02
2MASS 0908+5032	0.28	0.04	0.54	0.05	0.53	0.05
2MASS 0937+2931	0.78	0.05	1.37	0.06	-0.09	0.07
2MASS 0939-2448AB	0.81	0.06	1.87	0.06	-0.23	0.06
2MASS 1017+1308	0.18	0.04	0.33	0.03	0.35	0.04
2MASS 1047+2124	0.87	0.09	1.48	0.12	0.04	0.11
2MASS 1114-2618	0.79	0.04	1.76	0.05	-0.02	0.05
2MASS 1155-3727	0.16	0.02	0.32	0.03	0.33	0.03
2MASS 1204+3212	0.11	0.01	0.28	0.03	0.30	0.03
2MASS 1209-1004AB	0.6	0.11	0.83	0.10	0.34	0.10
2MASS 1217-0311	0.85	0.08	1.24	0.18	0.28	0.18
2MASS 1225-2739AB	1.00	0.10	1.6	0.04	0.51	0.04
2MASS 1237+6526	0.97	0.07	1.61	0.11	0.15	0.11
2MASS 1300+1912	0.10	0.02	0.23	0.04	0.27	0.04
2MASS 1439+1929	0.09	0.04	0.24	0.03	0.26	0.04
2MASS 1506+1321	0.17	0.03	0.28	0.02	0.27	0.06
2MASS 1507-1627	0.13	0.04	0.28	0.04	0.41	0.04
2MASS 1515+4847	0.24	0.03	0.48	0.03	0.5	0.03
2MASS 1526+2043	0.19	0.11	0.47	0.04	0.55	0.05
2MASS 1534-2952AB	0.90	0.07	1.27	0.09	0.35	0.09
2MASS 1546-3325	0.78	0.16	0.84	0.11	0.01	0.10

TABLE 7B – *Continued*

Name	$C_{[3.6\text{-}5.8\mu m]}$	σ_c	$C_{[3.6\text{-}8.0\mu m]}$	σ_c	$C_{[4.5\text{-}8.0\mu m]}$	σ_c
2MASS 1553+1532AB	1.12	0.10	1.77	0.10	0.43	0.10
2MASS 1555-0956	0.07	0.02	0.20	0.01	0.25	0.01
2MASS 1632+1904	0.46	0.06	0.70	0.06	0.65	0.06
2MASS 1645-1319	0.12	0.04	0.28	0.04	0.32	0.02
2MASS 1721+3344	0.09	0.04	0.18	0.03	0.22	0.03
2MASS 1728+3948AB	0.43	0.04	0.59	0.04	0.53	0.03
2MASS 1835+3259	0.16	0.02	0.26	0.02	0.26	0.01
2MASS 2104-1037	0.11	0.04	0.26	0.05	0.33	0.04
2MASS 2224-0158	0.20	0.04	0.24	0.04	0.33	0.04
2MASS 2244+2043	0.76	0.04	0.99	0.04	0.75	0.04
2MASS 2254+3123	0.90	0.10	1.15	0.10	0.50	0.10
2MASS 2339+1352	0.84	0.06	1.02	0.21	0.15	0.21
2MASS 2356-1553	1.12	0.09	1.48	0.17	0.48	0.17
BRI0021-0214	0.22	0.04	0.39	0.04	0.36	0.04
DEN0021-4244	0.19	0.04	0.32	0.04	0.29	0.04
DEN0255-4700	0.40	0.02	0.68	0.02	0.59	0.02
DEN1058-1548	0.16	0.04	0.26	0.04	0.27	0.04
DEN1539-0520	0.04	0.05	0.05	0.05	0.15	0.06
eps Ind BC	0.58	0.03	0.99	0.04	0.46	0.04
GJ-1001A	0.08	0.03	0.09	0.03	0.04	0.03
GJ-1001BC	0.22	0.03	0.23	0.02	0.34	0.02
GJ-1002	0.10	0.02	0.12	0.01	0.06	0.01
GJ-1093	0.10	0.03	0.12	0.03	0.10	0.02
GJ-1111	0.08	0.05	0.10	0.02	0.10	0.04
GJ-1156	0.14	0.03	0.16	0.03	0.08	0.02
GJ-337CD	0.54	0.08	0.55	0.05	0.38	0.05
GJ-412B	0.15	0.02	0.20	0.01	0.11	0.05
GJ-570D	1.03	0.12	1.83	0.08	0.15	0.07
GJ-644C	0.09	0.03	0.13	0.03	0.14	0.02
GJ-752B	0.14	0.02	0.15	0.02	0.16	0.03
GL 570D	1.03	0.12	1.83	0.09	0.15	0.08
HD 3651B	1.34	0.13	1.93	0.15	0.17	0.14
HN PegB	0.64	0.11	1.14	0.12	0.81	0.11
Kelu-1AB	0.19	0.07	0.31	0.07	0.29	0.06
LHS 102A	0.08	0.04	0.09	0.04	0.04	0.04
LHS 102BC	0.22	0.04	0.23	0.04	0.34	0.04
LHS 132	0.12	0.03	0.16	0.02	0.14	0.02
LHS 2021	0.08	0.02	0.12	0.02	0.15	0.01

TABLE 7B – *Continued*

Name	$C_{[3.6\text{-}5.8\mu m]}$	σ_c	$C_{[3.6\text{-}8.0\mu m]}$	σ_c	$C_{[4.5\text{-}8.0\mu m]}$	σ_c
LHS 2065	0.19	0.04	0.28	0.04	0.26	0.04
LHS 288	0.04	0.03	0.11	0.03	0.05	0.04
LHS 292	0.05	0.04	0.09	0.04	0.09	0.04
LHS 2924	0.19	0.04	0.35	0.04	0.35	0.04
LHS 3003	0.08	0.04	0.11	0.04	0.13	0.04
LP944-020	0.28	0.03	0.45	0.03	0.37	0.01
SDSS 0000+2554	1.16	0.09	1.22	0.04	0.57	0.04
SDSS 0151+1244	0.44	0.11	0.72	0.18	0.57	0.18
SDSS 0207+0000	0.92	0.21	1.42	0.20	0.81	0.20
SDSS 0423-0414AB	0.43	0.04	0.72	0.04	0.57	0.04
SDSS 0539-0059	0.14	0.05	0.29	0.06	0.40	0.06
SDSS 0758+3247	0.70	0.04	1.08	0.05	0.80	0.05
SDSS 0805+4812	0.12	0.04	0.34	0.04	0.33	0.04
SDSS 0837-0000	0.35	0.13	0.54	0.14	0.38	0.14
SDSS 0857+5708	0.60	0.04	0.88	0.04	0.70	0.04
SDSS 0926+5847AB	0.93	0.11	1.16	0.07	0.39	0.07
SDSS 1021-0304AB	0.58	0.12	1.00	0.11	0.64	0.11
SDSS 1052+4422AB	0.56	0.04	0.87	0.04	0.74	0.04
SDSS 1110+0116	1.28	0.08	1.50	0.16	0.67	0.16
SDSS 1155+0559	0.33	0.04	0.57	0.04	0.57	0.04
SDSS 1207+0244	0.44	0.04	0.63	0.07	0.50	0.07
SDSS 1254-0122	0.64	0.06	0.88	0.06	0.64	0.06
SDSS 1331-0116	0.01	0.09	0.34	0.07	0.51	0.07
SDSS 1346-0031	1.13	0.12	1.40	0.18	0.47	0.17
SDSS 1504+1027	1.07	0.05	1.68	0.08	0.25	0.08
SDSS 1516+3053	0.72	0.04	1.14	0.04	0.92	0.04
SDSS 1520+3546	0.45	0.04	0.68	0.04	0.63	0.04
SDSS 1624+0029	1.05	0.09	1.46	0.10	0.24	0.09
SDSS 1628+2308	1.11	0.06	1.70	0.08	0.31	0.08
SDSS 1750+1759	0.80	0.23	1.02	0.23	0.53	0.23
SDSS 2028+0052	0.14	0.04	0.26	0.04	0.32	0.04
SO 0253+1652	0.07	0.01	0.10	0.01	0.08	0.02
ULAS 0034-0052	1.46	0.06	2.37	0.07	0.58	0.07
ULAS 0857+0913	1.15	0.10	1.29	0.31	0.37	0.31
ULAS 1017+0118	1.39	0.05	1.59	0.15	0.32	0.15
ULAS 1238+0953	1.77	0.07	2.51	0.10	0.76	0.10
ULAS 1335+1130	1.61	0.06	2.58	0.07	0.54	0.07
ULAS 2146-0010	1.06	0.15	2.08	0.09	0.07	0.09

VIII. Appendix of Figures

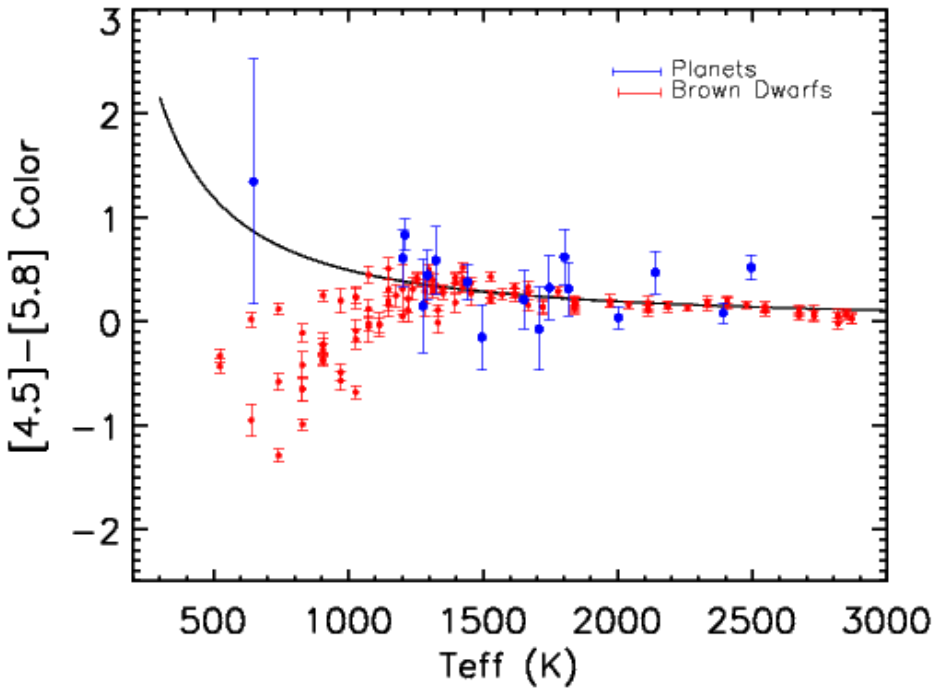

FIG. 10: [4.5μm]-[5.8μm] color versus effective temperature in K for known brown dwarfs (in red) and planets (in blue), as well as for a uniform blackbody model. Uncertainties in color for individual objects are shown, average uncertainties in temperature are shown on upper right. Plot is based on data shown in Table 4A, & 7A.

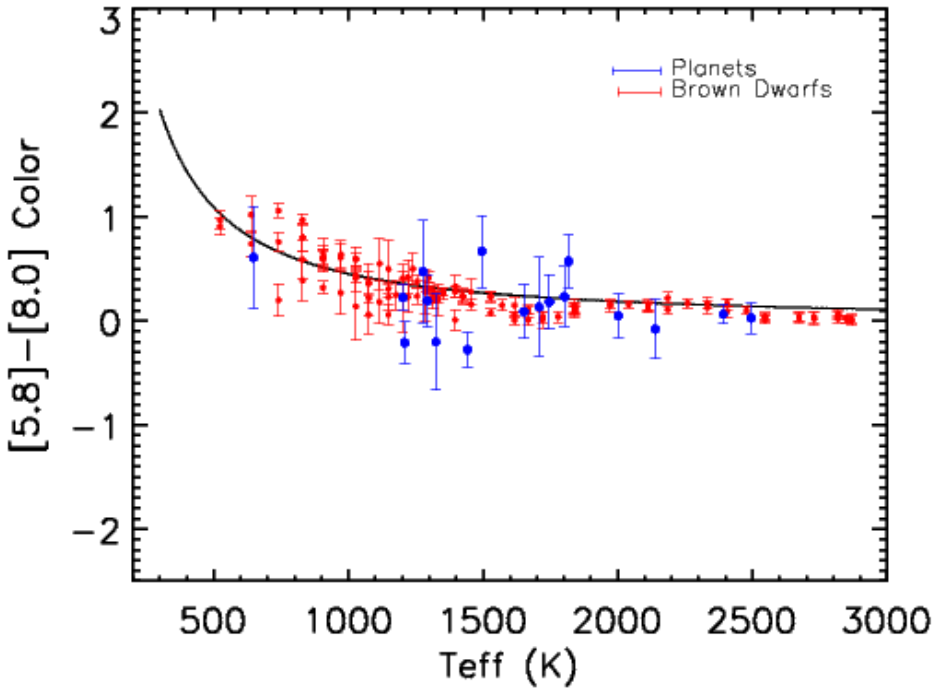

FIG. 11: [5.8μm]-[8.0μm] color versus effective temperature in K for known brown dwarfs and planets, as well as for a uniform blackbody model. Plot is based on data shown in Table 4A, & 7A.

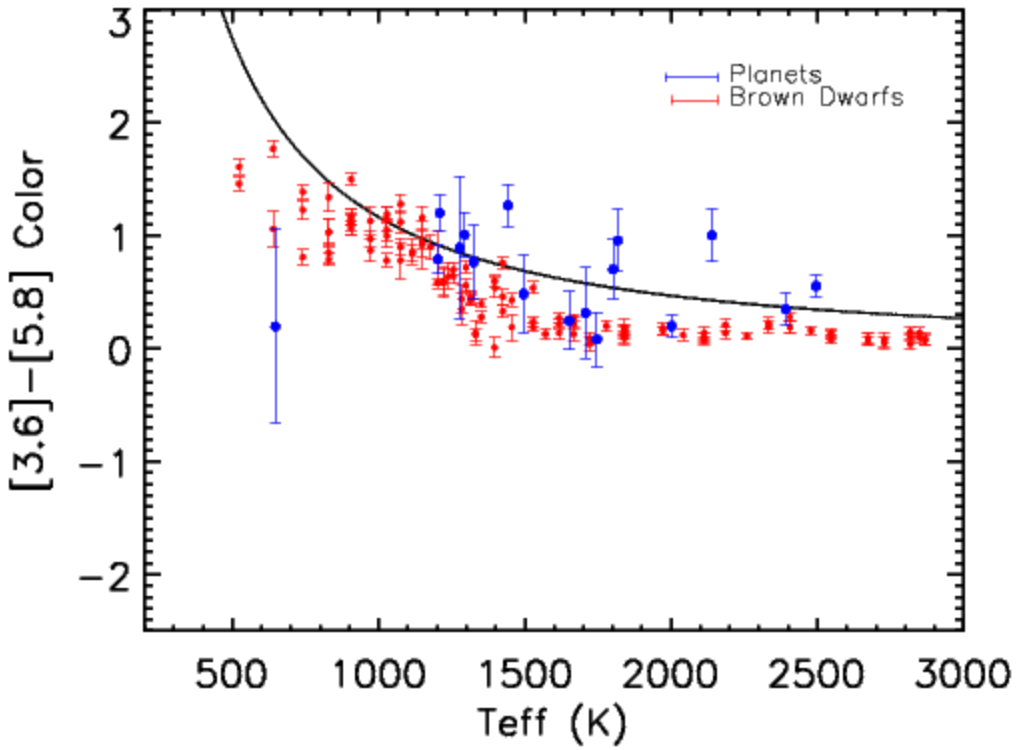

FIG. 12: [3.6μm]-[5.8μm] color versus effective temperature in K for known brown dwarfs and planets, as well as for a uniform blackbody model. Plot is based on data shown in Table 4B, 7A, & 7B.

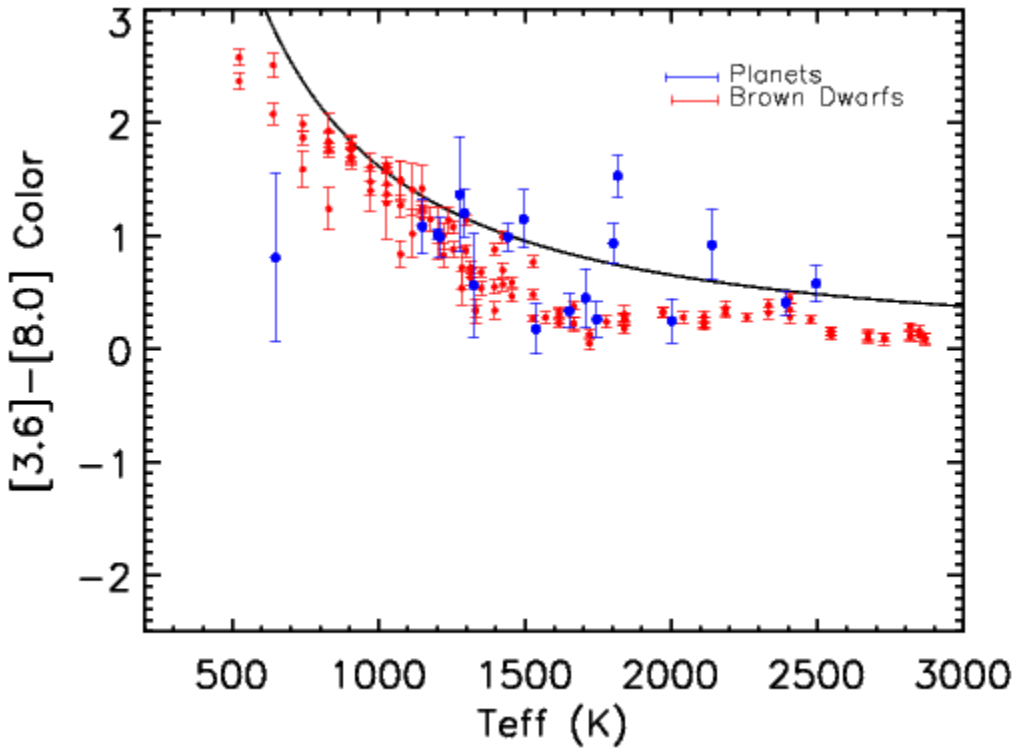

FIG. 13: [3.6μm]-[8.0μm] color versus effective temperature in K for known brown dwarfs and planets, as well as for a uniform blackbody model. Plot is based on data shown in Table 4B, 7A, & 7B.

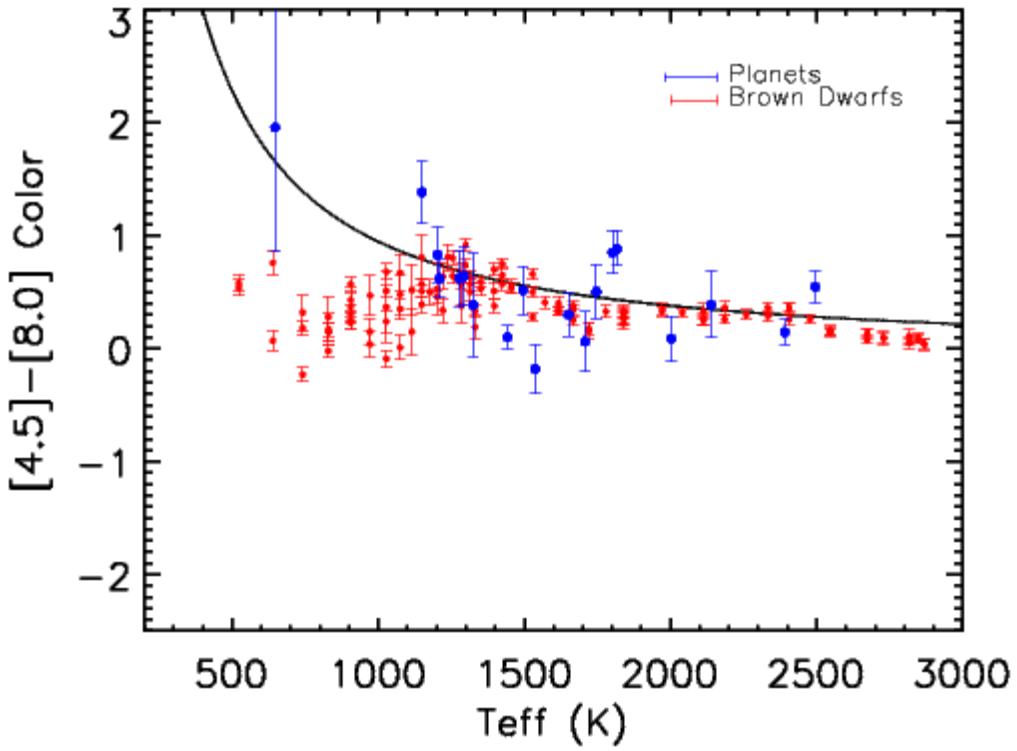

FIG. 14: [4.5μm]-[8.0μm] color versus effective temperature in K for known brown dwarfs and planets, as well as for a uniform blackbody model. Plot is based on data shown in Table 4B, 7A, & 7B.

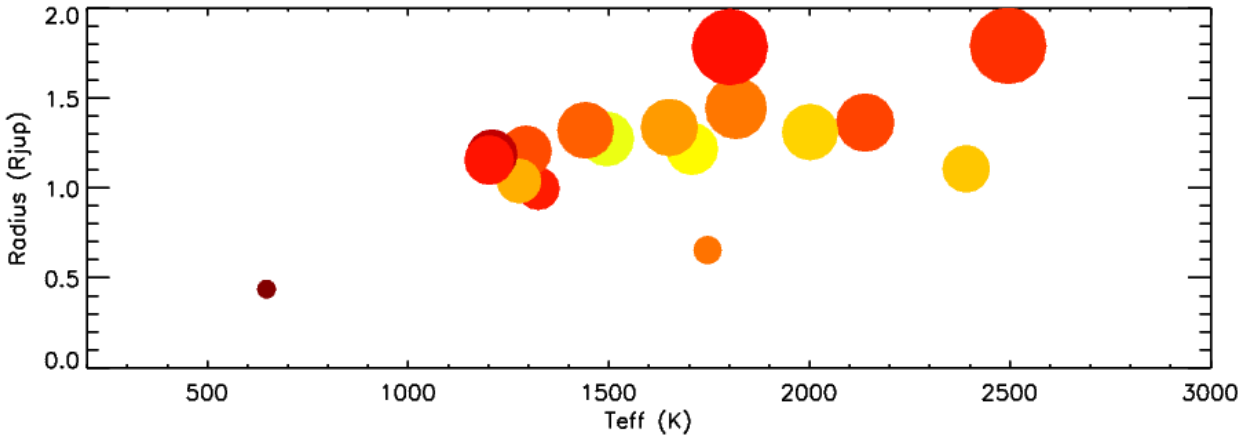

FIG. 15: Diversity plot for 17 planets. Planets are colored on a blue-to-red scale based on their [4.5μm]-[5.8μm] color and scaled based on their radius. Radius and color scales are the same as in Figure 8. Objects with more positive color on this case are redder, and those with more negative color are bluer (and would appear so to an observer viewing them on these infrared wavelengths). Plot is based on data in Tables 2 & 4A.

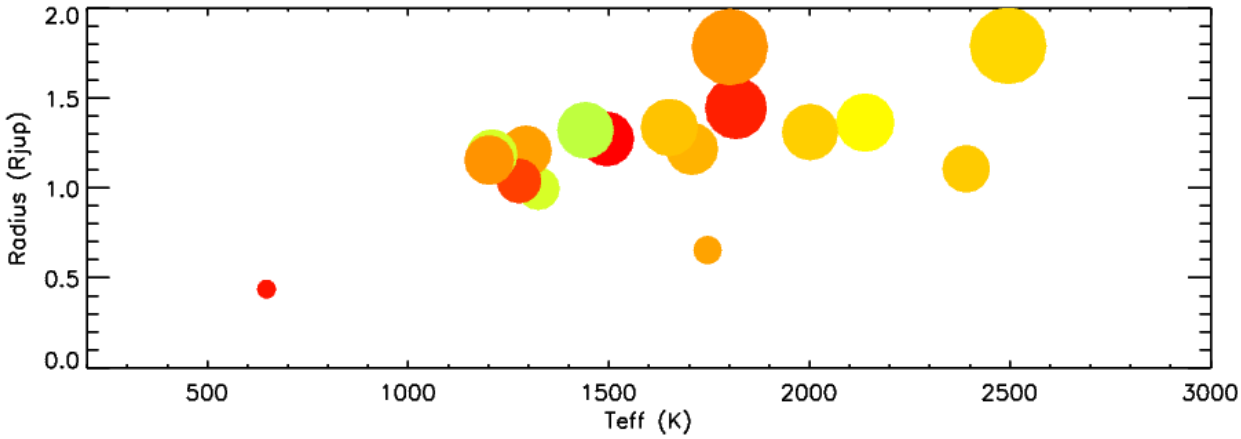

FIG. 16: Diversity plot for the same 17 planets as Figure 15. Planets are colored on a blue-to-red scale based on their [5.8μm]-[8.0μm] color and scaled based on their radius. Radius and color scales are the same as in Figure 8. Plot is based on data in Tables 2 & 4A.

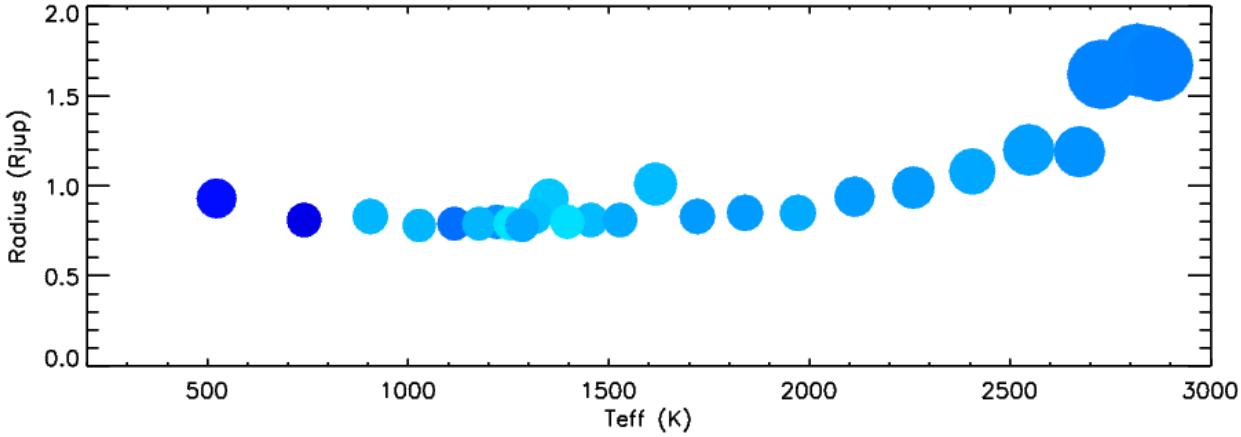

FIG. 17: Diversity plot for 27 brown dwarfs. These are also colored on a blue-to-red scale based on their [4.5μm]-[5.8μm] color and scaled based on their estimated radius, which is based on a brown dwarf model created by Baraffe et al. (2003). Radius and color scales are same as Figure 9. Plot is based on this model as well as data shown in Table 6 & 7A.

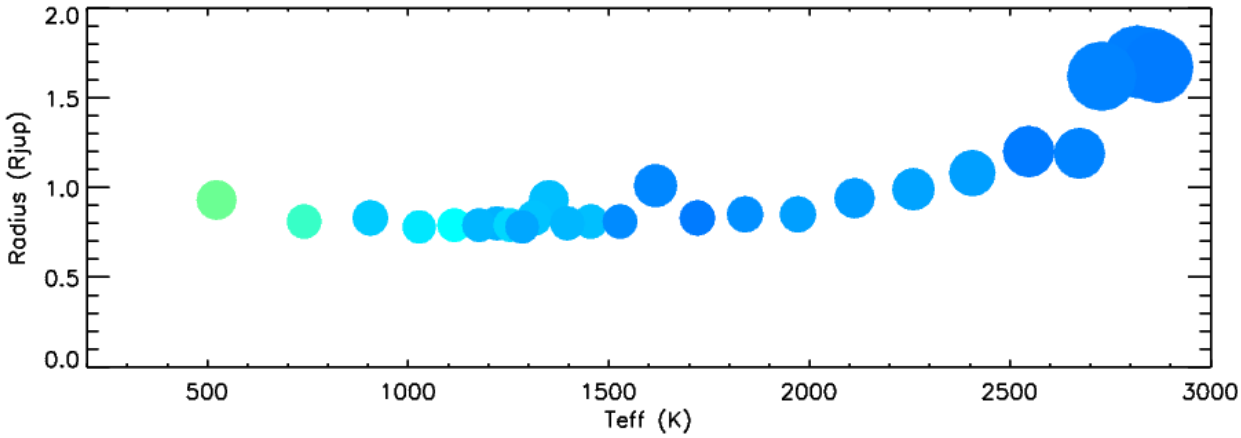

FIG. 18: Diversity plot for 27 brown dwarfs. These are also colored on a blue-to-red scale based on their [5.8μm]-[8.0μm] color and scaled based on their estimated radius. Radius and color scales are same as Figure 9. Plot is based on this model as well as data shown in Table 6 & 7A.

IX. References

Baraffe, I., Chabrier, G., Barman, T. S., Allard, F., & Hauschildt, P.H. 2003, A&A, 402, 701.

Boss, A. P. 2003. *Position Statement On The Definition Of A "Planet."* Working Group On Extrasolar Planets (WGESP) Of The IAU. 01 Dec 2011 <http://www.dtm.ciw.edu/boss/definition.html>.

Brown, M. E., Trujillo, C. A., & Rabinowitz, D. L. 2005, ApJ, 635, L97.

Brown, T. M. 2001, ApJ, 553, 1006.

Bruno, G. 1584, De l'Infinito Universo et Mondi. (Venice).

Burgasser, A. J., Tinney, C. G., Cushing, M. C., Saumon, D., Marley, M. S., Bennett, C. S., & Kirkpatrick, J. D. 2008, ApJ, 689, L53.

Burningham, B., *et al.* 2008, MNRAS, 391, 320.

Burrows, A., Hubbard, W. B., Lunine, J. I., & Leibert, J. 2001, Rev.Mod.Phys., 73, 719.

Centre National D'Etudes Spatiales 2006. *Constantly Stretching the Limits of the Universe.* 23 Feb 2012. <http://www.cnes.fr/web/CNES-en/1403-constantly-stretching-the-limits-of-the-universe.php>.

Charbonneau, D., Brown T. M., Latham, D. W., & Mayor, M. 1999, ApJ, 529, L45.

Charbonneau, D., Brown T. M., Burrows, A., & Laughlin., G. 2007, review chapter in *Protostars and Planets V*, eds. D. Jewitt & B. Reipurth, (Tuscon: U. Arizona Press).

Deleuil, M., *et al.* 2008, A&A, 491, 889.

De Pater, I., & Lissauer, J. J., 2001, Planetary Sciences. (Cambridge: Cambridge U. Press).

Gibori, B., & Brown, M. E. 2006, AREPS, 34, 193.

Hansen, B.M.S., & Barman, T. 2007, ApJ, 681, 861.

International Astronomical Union. 2006. *Resolution B5: Definition of a Planet in the Solar System*. IAU Resolutions. 01 Dec 2011 <http://www.iau.org/static/resolutions/Resolution_GA26-5-6.pdf>.

Feagley, B., & Lodders, K. 1996, ApJ, 472, L37.

Fortney, J. J., Lodders, K., Marley, M. S., & Freedman, R. S. 2008, ApJ, 678, 1419.

Kipping, D. & M., Spiegel, D. S. 2011, MNRAS, 417, L88.

Kirkpatrick, J. D., *et al.* 2011, ApJS, 197, 19.

Leggett, S. K., *et al*. 2010, ApJ, 710, 1627.

Line, M. R., Vasisht, G., Chen, P., Angerhausen, D., & Yung, Y. L. 2011, ApJ, 738, 32.

Linsky, J. L., *et al*. 2010, ApJ, 717, 1291.

Lodders, K. 2004, Science 303, 323.

Lodders, K., & Fegley, B. Jr., 2006, Astrophysics Update, 2, 1-28.

Luhman, K. L., *et al.* 2007, ApJ, 654, 570.

Luhman, K. L., *et al.* 2012, ApJ 744, 135.

NASA/JPL/Space Science Institute, 2003. *PIA04866: Cassini Jupiter Portrait*. NASA Planetary Photojournal. 02 Dec 2011<http://photojournal.jpl.nasa.gov/catalog/pia04866>.

O'Donovan, F. T., *et al.* 2006, ApJ, 651, L61.

Patten, B. M., *et al.* 2006, ApJ, 651, 502.

Schneider, J., Dedieu, C., Le Sidaner, P., Savalle, R., & Zolotukhin, I. 2011, A&A, 532, A79.

Seager, S., Richardson, L. J., Hansen, B. M. S., Menou, K., Cho, J. Y.-K., & Deming, D. 2005, ApJ, 632,1122.

Seager, S., & Deming, D. 2010, ARAA, 48, 631.

Stephens, D. C., *et al.* 2009, ApJ, 702, 154.

Stevenson, K. B., *et al*.2010, Nature, 464, 1161.

Warren, S. J., *et al.* 2007, MNRAS, 381, 1400.

Winn, J. N. 2010, chapter of *Exoplanets*, ed. Sara Seager, (Tuscon: U. Arizona Press).

X. References For Data Tables

Albrecht, S., *et al.* 2011, ApJ, 738, 50.

Alonso, R., *et al.* 2004, ApJ, 613, L153.

Alonso, R., *et al.* 2008, A&A, 482, L21.

Baines, E. K., *et al.* 2008, ApJ, 680, 728.

Bakos, G. Á., *et al.* 2007a, ApJ, 656, 552.

Bakos, G. Á., *et al.* 2007b, ApJ, 671, L173.

Barge, P., *et al*. 2008, A&A, 482, L17.

Basri, G., *et al.* 2000, ApJ, 538, 363.

Bean, J. L., *et al.* 2008, A&A, 1039.

Beaulieu, J. P., *et al.* 2011, ApJ, 731, 16.

Beerer, I. M., *et al.* 2011, ApJ, 727, 23.

Belle, G. T. 2008, ASP, 120 (868), 617.

Bessell, M. S. 1991, AJ, 101, 662.

Bidelman, G. P. 1985, ApJS, 59, 197.

Bonomo, A. S., *et al*. 2012, A&A, 538, A96.

Borucki, W.J., *et al.* 2010, Science, 327, 977.

Bouchy, F., *et al.* 2008, A&A, 482, L25.

Brown, T. M. 2001, ApJ, 553, 1006.

Burgasser, A. J., Geballe, T. R., Leggett, S. K., Kirkpatrick, J. D., & Golimowski, D. A. 2006, ApJ, 637, 1067.

Burgasser, A. J., Kirkpatrick, J. D., Reid, I. N., Brown, M. E., Miskey, C. L., & Gizis, J. E. 2003, ApJ, 586, 512.

Burgasser, A. J., Reid, I.N., Leggett, S. K., Kirkpatrick, J. D., Leibert, J., & Burrows, A. 2005, ApJ, 634, L177.

Burgasser, A. J., Tinney, C. G., Cushing, M. C., Saumon, D., Marley, M. S., Bennett, C. S., & Kirkpatrick, J. D. 2008, ApJ, 689, L53.

Burke, C. J., *et al.* 2007, ApJ, 671, 2115.

Burningham, B., *et al.* 2008, MNRAS, 391, 320.

Burningham, B., *et al.* 2009, MNRAS, 395, 1237.

Burningham, B., *et al.* 2010, MNRAS, 406, 1885.

Cáceres, C., *et al.* 2009, A&A, 507, 481.

Cameron, C. A., *et al.* 2007a, MNRAS, 375, 951.

Cameron, C. A., *et al.* 2007b, MNRAS, 380, 1230.

Chan, T., Ingemyr, M., Winn, J. M., Holman, M. J., Sanchis-Ojeda, R., Esquerdo, G., & Everett, M. 2011, ApJ, 141, 179.

Charbonneau, D., *et al.* 2005, ApJ, 626, 523.

Charbonneau, D., *et al.* 2008, ApJ, 686, 1341.

Chiu, K., *et al.* 2006, AJ, 131, 2722.

Chiu, K., *et al.* 2008, MNRAS, 385, L35.

Christiansen, J. L., *et al*. 2010, ApJ, 710, 97.

Christiansen, J. L., *et al*. 2011, ApJ, 726, 96.

Cowan, N. B., *et al.* 2012, ApJ, 747, 82.

Cruz, K. L., Reid, I. N., Liebart, J., Kirkpatrick, J. D., & Lowrance, P. J., AJ, 126, 2421.

Daemgen, S., Hormuth, F., Brandner W., Bergfors, C., Janson, M., Hippler, S., & Henning, T. 2009, A&A, 498, 567.

Deming, D., *et al.* 2011, ApJ, 726, 95.

Désert, J-M., *et al*. 2011a, ApJS, 197, 11.

Désert, J-M., *et al*. 2011b, ApJS, 197, 14.

Dunham, E. W., *et al.* 2010, ApJ, 713, L136.

Fortney, J. J., *et al.* 2011, ApJS, 197, 9.

Fressin, F., *et al.* 2010, ApJ, 711, 374.

Geballe, T. R., *et al.* 2002, ApJ, 564, 466.
Gizis, J. E., 2002, ApJ, 575, 484.
Gizis, J. E., Monet, D. G., Reid, I. N., Kirkpatrick, J. D., Liebert, J., & Williams, R. J. 2000, ApJ, 120, 1085.
Golimowski, D. A., *et al.* 2004, AJ, 127, 3516.
Hawley, S. L., *et al.* 2002, AJ, 123, 3409.
Hebb, L., *et al.* 2010, ApJ, 708, 224.
Hellier, C., *et al.* 2009, Nature, 460, 1098.
Hellier, C., *et al.* 2011, ApJ, 730, L31.
Henry, T. J., *et al.* 1999, ApJ, 512, 864.
Henry, T. J., Subasavage, J. P., Brown, M. A., Beaulieu, J. P., Jao, W.-C., & Hambly, N. C. 2004, AJ, 128, 2460.
Holman, M. J., *et al.* 2006, ApJ, 654, 1715.
Johnson, J. A., *et al.* 2008, ApJ, 686, 649.
Joshi, Y. C., *et al.* 2008, MNRAS, 392, 1532.
Kirkpatrick, J. D., Barman, T. S., Burgasser, A. J., McGovern, M. R., McLean, I. S., Tinney, C. G., & Lowrance, P. J. 2006, ApJ, 639, 1120.
Kirkpatrick, J. D., Beichman, C. A., Skrutskie, M. F., 1997, ApJ, 476, 311.
Kirkpatrick, J. D., Dahn, C. C., Monet, D. G., Reid, I. N., Gizis, J. E., Liebert, J., & Burgasser, A. J. 2001, AJ, 121, 3235.
Kirkpatrick, J. D., Henry, T. J., & McCarthey, D. W., Jr. 1991, ApJS, 77, 417.
Kirkpatrick, J. D., *et al.* 1999, ApJ, 519, 802.
Kirkpatrick, J. D., *et al.* 2000, AJ, 120, 447.
Kirkpatrick, J. D., *et al.* 2011, ApJS, 197, 19.
Knapp, G. R., *et al.* 2004, AJ, 127, 3553.
Knutson, H., Charbonneau, D., Allen, L. E., Burrows, A., & Megeath, S. T. 2008, ApJ, 673, 526.
Knutson, H., Charbonneau, D., Burrows, A., O'Donovan, F. T., & Mandushev, G. 2009, ApJ, 691, 866.
Latham, D. W., *et al.* 2009, ApJ, 704, 1107.
Leggett, S. K. 1992, ApJS, 82, 351.
Leggett, S. K., Saumon, D., Marley, M. S., Geballe, T. R., Golimowski, D. A., Stephens, D., & Fan, X. 2007, ApJ, 655, 1079.
Leggett, S. K., *et al.* 2010, ApJ, 710, 1627.
Luhman, K. L., *et al.* 2007, ApJ, 654, 570.
Luhman, K. L., *et al.* 2012, ApJ 744, 135.
Machalek, P., McCullough, P. R., Burke, C. J., Valenti, J. A., Burrows, A., & Hora, J. L. 2008, ApJ, 684, 1427.
Machalek, P., McCullough, P. R., Burrows, A., Burke, C. J., Hora, J. L., & Johns-Krull, C. M. 2009, ApJ, 701, 514.
Machalek, P., *et al.* 2010, ApJ, 711, 111.
Madhusudhan, N., *et al.* Nature, 469, 64.
McCullough, P. R., *et al.* 2006, ApJ, 648, 1228.
McCullough, P. R., *et al.* 2008, ApJ, submitted.
Moutou, C., *et al.* 2011, A&A, 533, A113.
Narita, N., Hirano, T., Sato, B., Harakawa, H., Fukui, A., Aoki, W., & Tamura, M. 2011, PASJ, in press.
Nordström, B., *et al.*2004, A&A, 418, 989.
Noyes, R. W., *et al.* 2008, ApJ, 673, L79.
Nutzman, P., Charbonneau, D., Winn, J. N., Knutson, H., Fortney, J. J., Holman, M. J., & Agol, E. 2009, ApJ, 692, 229.
Nymeyer, S., *et al.* 2011, ApJ, 742, 35.
O'Donovan, F. T., *et al.* 2007, ApJ, 663, L37.
O'Donovan, F. T., Charbonneau, D., Harrington, J., Madhusudhan, N., Seager, S., Deming, D., & Knutson, H. 2010, ApJ, 710, 1551.
Pál, A. 2012, MNRAS, submitted.
Pál, A., *et al.* 2008, ApJ, 680, 1450.
Patten, B. M., *et al.* 2006, ApJ, 651, 502-516.
Raetz, St., *et al.* 2009, Astron. Nachr., 330, 475.
Reid, I., *et al.* 2003, AJ, 125, 354.
Sanchis-Ojeda, R., Winn, J. N., Holman, M. J., Carter, J. A., Osip, D. J., & Fuentes, C. I. 2011, ApJ, 733, 127.
Santos, N. C., Israelian, G., Mayor, M., Rebolo, R., & Udry, S. 2003, A&A, 398, 363.
Sato, B., *et al.* 2005, ApJ, 633, 465.
Scholz, R.-D., Irwin, M., Ibata, R., Jahreiss, H., & Malkov, O. Y., A&A, 353, 958.
Schröter, J. H., Schmitt, M. M., & Müller, H. M. 2012, A&A, 539, A97.
Schuler, S. C., Flateau, D., Cunha, K., King, J. R., Ghezzi, L., & Smith, V. V., ApJ, 732, 55.
Southworth, J. 2008, MNRAS, 386, 1644.
Southworth, J. 2010, MNRAS, 408, 1689.
Southworth, J., *et al.* 2009, ApJ, 707, 167.
Southworth, J., *et al.* 2012, MNRAS, 422, 3099.
Sozzetti, A., *et al.* 2007a, ApJ, 664, 1190.
Sozzetti, A., *et al.* 2007b, IAU Symposium, 249, 261.
Stempels, H. C., Cameron, A. C., Hebb, L., Smalley, B., & Frandsen, S. 2007, MNRAS, 379, 773.
Stevenson, K. B., *et al.*2010, Nature, 464, 1161.
Stevenson, K. B., *et al.*2011, ApJ, submitted.
Todorov, K., *et al.* 2010, ApJ, 708, 498.
Todorov, K., *et al.* 2012, ApJ, 746, 111.
Torres, G. 2007, ApJ, 671, L65.
Torres, G., Winn, J. N., & Holman, M. J. 2008, ApJ, 677, 1324.
Triaud, A. H. M. J., *et al.* 2010, A&A, 524, A25.
Warren, S. J., *et al.* 2007, MNRAS, 381, 1400.
Wheatley, P. J., *et al.* 2010, ApJ, submitted.
Wilson, D. M., *et al.* 2008, ApJ, 675, L113.
Wilson, J. C., Kirkpatrick, J. D., Gizis, J. E., Skrutskie, M. F., Monet, D. G., & Houck, J. R. 2001, AJ, 122, 1989.
Wilson, J. C., *et al.* 2003, IAU Symposium, 211, 197.
Winn, J. N., *et al.* 2008, ApJ, 683, 1076.